HHS Public Access

Author manuscript

Sci Immunol. Author manuscript; available in PMC 2024 January 18.

Published in final edited form as:

Sci Immunol. 2023 September 08; 8(87): eadf4968. doi:10.1126/sciimmunol.adf4968.

Pre-existing tumor-resident T cells with cytotoxic potential associate with response to neoadjuvant anti-PD-1 in head and neck cancer

Giacomo Oliveira[1,2,†], **Ann Marie Egloff**[1,2,3,†], **Alexander B. Afeyan**[1,2,†], **Jacquelyn O. Wolff**[4], **Zexiang Zeng**[1], **Rebecca D. Chernock**[5], **Liye Zhou**[1], **Cameron Messier**[1,6], **Patrick Lizotte**[1,6], **Kathleen L Pfaff**[4], **Kari Stromhaug**[1], **Livius Penter**[1,2,7,8], **Robert I. Haddad**[1,9], **Glenn J. Hanna**[1,9], **Jonathan D. Schoenfeld**[10], **Laura A. Goguen**[3], **Donald J. Annino**[3], **Vickie Jo**[11], **Peter Oppelt**[12,13], **Patrik Pipkorn**[14], **Ryan Jackson**[14], **Sidharth V. Puram**[14], **Randal C. Paniello**[14], **Jason T. Rich**[14], **Jason Webb**[1], **Jose P. Zevallos**[1], **Mena Mansour**[5], **Jingxin Fu**[1],

[*]Correspondence should be addressed to: Ravindra Uppaluri, MD/PhD or Catherine J. Wu, MD, Dana-Farber Cancer Institute, 450 Brookline Avenue, Boston MA 02215, Ravindra_Uppaluri@DFCI.HARVARD.EDU, cwu@partners.org.

[†]Equal contribution

[‡]Co-senior authors

Author Contributions: R.U., D.R.A., A.M.E, G.O. and C.W. designed the study and wrote the manuscript. G.O., A.B.A., Z.Z., J.F., L.Z., K.S. and L.P. performed the bioinformatic analyses. D.K., J.F.P. and A.M.E. performed the statistical analysis of the clinical data. R.D.C., M.M. and V.J. assessed the pathological response of the tumor samples. A.M.E., R.U., J.W., C.M. C.P.P. and P.L. collected and processed tumor specimens. J.O.W., K.L.P. and S.J.R. performed and analyzed immunofluorescence. J.L. and A.M.E. managed the clinical data. R.U., D.R.A., J.P.Z., S.V.P., R.C.P., J.T.R., R.J., P.P, D.J.A., L.A.G., J.D.S., G.P.D, G.J.H., R.I.H., P.O., L.D. and L.G.T.M. were responsible for clinical management. All authors critically revised the manuscript.

Competing interests: G.J.H. reports grants from Bristol Myers Squibb during the conduct of the study as well as grants and personal fees from Bicara, Exicure, Regeneron, BMS, and Sanofi Genzyme; grants from Gateway for Cancer Research, GSK, Kite Pharma, NantKwest/Altor Bioscience, and Secura Bio; and personal fees from Maverick and Merck outside the submitted work. V.Y.J. reports "my spouse works as a Principal Scientist at Merck and Co for which he receives a salary, but his line of work in non-oncology has no relevant conflicts with this present study." C.P.P. reports Stock and Other Ownership Interests: XSphera Biosciences, Honoraria from Bio-Rad, Consulting or Advisory Role: DropWorks and XSphera Biosciences, Sponsored research agreements with Daiichi Sankyo, Bicycle Therapeutics, Transcenta, Bicara Therapeutics, AstraZeneca, Intellia Therapeutics, Janssen Pharmaceuticals, Array Biopharma, Takeda, KSQ therapeutics, Ideya Biosciences, BOLT therapeutics, Lilly Pharmaceuticals, Thermo Fisher Scientific and Bristol Myers Squibb. J.D.S. reports grants from BMS during the conduct of the study as well as grants from Merck, Merck KGA, BMS, Regeneron, and Debiopharm and personal fees from Castle Biosciences, Merck KGA, Genentech, Immunitas, Debiopharn, LEK, Catenion, ACI Clinical, Astellas, and Stimit outside the submitted work and equity in Doximity and Immunitas. R.I.H. reports grants from BMS during the conduct of the study as well as grants and personal fees from Merck, BMS, Pfizer, GSK, Merck Serono, Eisai, Bayer, AstraZeneca, Kura, NCCN, Nanobiotix, ISA, and Mirati outside the submitted work. R.D.C. reports personal fees from Roche (Advisory Board Member) and Merck (Consultant) during the conduct of the study, as well as a non-financial relationship with Caris Life Sciences as a member of their Precision Oncology Alliance. D.R.A. reports grants and personal fees from Merck (research funding and advisory board) during the conduct of the study; Pfizer (research funding and advisory board), Eli Lilly (research funding and advisory board), Celgene - now BMS (research funding and advisory board), Cue Biopharma (research funding and advisory board), personal fees from Loxo Oncology (advisory board), grants from Novartis (research funding), Roche (research funding), Aduro (research funding), Atara (research funding), Matrix (research funding), Blueprint Medicine (research funding), Celldex (research funding), Enzychem (research funding), Exilixis (research funding), Shanghai De Novo (research funding), Kura (research funding), Astrazeneca (research funding), Medimmune (research funding), and Innate (research funding) outside the submitted work. J.P.Z. is a founder and equity shareholder of Droplet Biosciences (Cambridge, MA), equity shareholder of Summit Biolabs (Aurora, CO) and consultant for Merck. C.J.W. is an equity holder of BioNTech (outside the submitted work). R.U. reports grants and personal fees from Merck Inc. The remaining authors declare no competing interests.

Data and material availability: Single-cell RNA and TCR sequencing are available through the dbGAP accession phs002864.v1.p1. Previously published scRNA-seq data reanalyzed here are referenced within the Material and Method section. All other raw data needed to support the conclusions of the paper are present in the paper or the Supplementary Materials or have been previously published (3, 30). Code used for data analysis is available from previous publications(14, 24) and included Salmon (for RNA-seq analysis), Cell Ranger v3.0.2 (for single cell-data alignment), Seurat v4.1.0 (single-cell sequencing analysis), Harmony v1.0 (single-cell data normalization), SingleR v1.4.1 and scater v1.18.6, (for comparison with other single cell datasets), and FGSEA v1.16.0 (for gene set enrichment analysis) and are each publicly available.

List of Supplementary Materials

Supplementary Materials is available for this paper at the end of the document or at linked Excel files and includes:

Gavin P. Dunn[15], **Scott J. Rodig**[9,11], **Jessica Ley**[12,13], **Luc G.T. Morris**[16], **Lara Dunn**[17], **Cloud P. Paweletz**[1,6], **Dorina Kallogjeri**[14], **Jay F. Piccirillo**[14], **Douglas R. Adkins**[12,13,‡], **Catherine J. Wu**[1,2,7,9,‡,*], **Ravindra Uppaluri**[1,2,3,‡,*]

[1]Department of Medical Oncology, Dana-Farber Cancer Institute, Boston, MA, USA

[2]Harvard Medical School; Boston, MA, USA.

[3]Department of Surgery, Brigham and Women's Hospital, Boston, MA, USA

[4]Center for Immuno-Oncology, Dana-Farber Cancer Institute; Boston, MA, USA

[5]Department of Pathology and Immunology, Washington University School of Medicine; St. Louis, MO, USA

[6]Belfer Center for Applied Cancer Science, Dana-Farber Cancer Institute; Boston, MA, USA

[7]Broad Institute of MIT and Harvard, Cambridge, MA, USA

[8]Department of Hematology, Oncology and Tumor immunology, Campus Virchow Klinikum, Berlin, Charité - Universitätsmedizin Berlin, corporate member of Freie Universität Berlin and Humboldt-Universität zu Berlin, Berlin, Germany.

[9]Department of Medicine, Brigham and Women's Hospital, Boston, MA, USA

[10]Department of Radiation-Oncology, Brigham and Women's Hospital; Boston, MA, USA

[11]Department of Pathology, Brigham and Women's Hospital; Boston, MA, USA

[12]Alvin J. Siteman Cancer Center, Washington University School of Medicine, St. Louis, MO, USA

[13]Department of Medicine/Medical Oncology, Washington University School of Medicine, St. Louis, MO, USA

[14]Department of Otolaryngology, Washington University School of Medicine; St. Louis, MO, USA

[15]Department of Neurological Surgery, Massachusetts General Hospital; Boston, MA, USA

[16]Department of Surgery, Memorial Sloan Kettering Cancer Center, New York, New York, USA.

[17]Department of Medical Oncology, Memorial Sloan Kettering Cancer Center, New York, New York, USA.

Abstract

Approximately 50% of patients with locally advanced head and neck squamous cell carcinoma (HNSCC) experience recurrences after definitive therapy. The pre-surgical administration of anti-PD-1 immunotherapy results in significant pathologic tumor responses (pTR) within the tumor microenvironment (TME). However, the mechanisms underlying the dynamics of antitumor T cells upon neoadjuvant PD-1 blockade remain unresolved and approaches to increase pathologic responses are lacking. In a phase II trial (NCT02296684), we observed that 45% of patients treated with two doses of neoadjuvant pembrolizumab experienced marked pTRs (≥50%). Single cell analysis of 17,158 CD8+ T cells from 14 tumor biopsies, including 6 matched pre-post neoadjuvant treatment, revealed responding tumors had clonally expanded putative tumor-specific exhausted CD8+ TILs with a tissue-resident memory program, characterized by high cytotoxic potential (CTX+) and *ZNF683* expression, within the baseline TME. Pathologic

responses following five weeks of PD-1 blockade were consistent with activation of pre-existing CTX+*ZNF683*+CD8+ TILs, paralleling loss of viable tumor and associated tumor antigens. Response was associated with high numbers of CD103+PD−1+ CD8+ T cells infiltrating pre-treatment lesions, while revival of non-exhausted persisting clones and clonal replacement were modest. By contrast, non-responder baseline TME exhibited relative absence of *ZNF683*+CTX+ TILs and subsequent accumulation of highly exhausted clones. In HNSCC, revival of pre-existing *ZNF683*+CTX+ TILs is a major mechanism of response in the immediate post-neoadjuvant setting.

One Sentence Summary

Neoadjuvant anti-PD-1 HNSCC response associates with revival of pre-existing TILs with cytotoxic potential and resident memory program.

Introduction

Head and neck squamous cell carcinoma (HNSCC) is the seventh most common type of cancer worldwide (1). A substantial number of patients with HNSCC develop recurrent and/or metastatic disease despite intensive multimodality treatment. Approval of programmed cell death protein 1 (PD-1) targeting agents has transformed the care of patients with recurrent and/or metastatic disease. With these successes, numerous trials are now exploring PD-1 targeting in the initial management of locally advanced HNSCC, including neoadjuvant treatment prior to ablative surgery. These approaches aim to induce *in situ* anti-tumor responses in order to enhance disease control in combination with standard surgical-based therapy. Although provocative tumor responses have been observed in multiple trials (2), the optimal schedule of neoadjuvant anti-PD-1 therapy and the immune mechanisms underlying tumor responses remain to be defined.

Neoadjuvant immunotherapy has been observed to result in pathologic tumor response (pTR) in 40-50% of patients with human papillomavirus (HPV) unrelated HNSCC (3-8), the most common and aggressive type of HNSCC. We previously reported that administration of neoadjuvant anti-PD-1 yielded better clinical outcomes than expected with surgery-based therapy alone (3). Major (<10% viable residual tumor, MPR) or complete pTR (CPR) were rarely seen in HNSCCs with single agent anti-PD-1 but we observed pTR with ≥50% tumor necrosis in the resection bed in 8 of 36 (22.2%) patients after a single dose of neoadjuvant pembrolizumab administered 2-3 weeks before surgery. An additional 22% of patients had pTR with 10-49% tumor necrosis in the resection bed (3). Although MPRs/CPRs were rare, recent data supports that HNSCC patients with even partial pTRs have improved clinical outcomes (4). These early data and other studies raised the question of whether an extended duration of anti-PD-1 therapy could further improve the pTR rate.

Numerous studies have revealed that the antitumor activity of anti-PD-1 treatment relies on the disruption of inhibitory signals in tumor infiltrating lymphocytes (TILs), leading to their functional reinvigoration. The dynamics of antitumor responses after immune checkpoint blockade are increasingly appreciated to differ based on cancer tissue of origin. Indeed, initial findings in melanoma patients responding to anti-PD-1 therapy revealed anti-PD-1

acts on existing clonotypes through induction of a single proliferative burst of circulating exhausted T cells (9). Response to PD-1 blockade for NSCLC and melanoma (10) has been associated with ‘clonal revival’ of pre-existing TILs, which can lead to the accumulation of less exhausted T cells within the TME, but this is not consistently observed for anti-PD-1-responsive patients with basal cell (BCC) or cutaneous squamous cell carcinoma (cSCC) (11). Possible alternate mechanisms of response in tumors with such moderate T cell infiltration might, for example, entail ‘clonal replacement’ of intratumoral T cells, since novel T cell clones have been reported to be recruited to the TME from lymph nodes and adjacent healthy tissues in these tumor settings.

For HNSCC, the mechanisms and cell types governing immunotherapy response are only beginning to be understood. A recent analysis of neoadjuvant PD-1 or combined PD-1/CTLA-4 blockade showed an early expansion of intra-tumoral CD8+ tissue resident memory cells and blood-derived clonotype expansion specifically following combination therapy. However, TME cellular dynamics in responder versus non-responder patients were not explored (12). Herein, we focused on the analysis of surgical specimens collected from a multicenter phase 2 clinical trial aimed at determining the impact of administering two doses of neoadjuvant pembrolizumab over 5 weeks before surgery in patients with resectable locally advanced HPV-unrelated HNSCC. Since tumor specimens were consistently collected at baseline, prior to any treatment, and at surgical resection following uniform neoadjuvant treatment, we had the valuable opportunity to evaluate the evolving immune T cell activation status and clonal dynamic differences between patients with and without pTR following pembrolizumab. Our single cell profiling-based studies of serial tumor specimens suggest reinvigoration of exhausted tissue resident memory cytotoxic tumor-infiltrating T lymphocytes rather than newly infiltrating clonotypes as major effectors of early response to neoadjuvant PD-1 blockade in HNSCC.

Results

Responses upon extended administration of neoadjuvant anti-PD-1 therapy

We previously reported a multicenter phase 2 clinical trial (Cohort 1) where HNSCC patients received one dose of anti-PD-1 prior to surgery (3). Herein, we report on Cohort 2 of this trial where thirty patients with stage III/IV HPV-unrelated HNSCC (Table 1) were enrolled and received two doses of the anti-PD-1 antibody pembrolizumab as neoadjuvant immunotherapy over 5 weeks prior to surgery (Fig. 1A). Patients had oral cavity, hypopharynx or larynx tumors, were predominantly male (63%) and most had a history of smoking (63%), typical of patients with HPV-unrelated HNSCC (Table 1, Table S1). Adverse events (AEs) possibly related to neoadjuvant pembrolizumab occurred in 9 of 30 patients (30%), with only one grade 3 AE (rash) that was therapy-related (Tables S2 and S3). There were no surgical delays or unexpected peri-surgical complications.

Baseline and restaging CT scans following neoadjuvant pembrolizumab and before surgery were performed for 29 patients. Tumor responses assessed by RECIST (modified v1.1, see Materials and Methods) included 1 complete response (CR), 4 partial responses (PR), 17 with stable disease (SD) and 7 with progressive disease (PD) (Fig. S1). Observed RECIST response did not impact the extent of surgery. Surgical resection was performed a median

of 40 days following the first dose of pembrolizumab (range 33-50 days) for twenty-nine patients.

The one-year relapse-free rate was 92.6% (95% CI: 73.5 – 98.1%) for the 29 two-dose patients who underwent surgical resection. Two-year overall survival (OS) and progression-free survival (PFS) rates were 92.44% (95% CI: 73.0-98.1) and 88.7% (95% CI: 68.9-96.2%), respectively (Fig. 1B). OS and PFS did not differ by pTR status (pTR-1/-2 vs. pTR-0) (p=0.956 and p=0.517, respectively, log rank test) during this initial follow-up period. Further AE and surgical timing details are presented in Supplementary Results.

pTR to PD-1 blockade was assessed based on histologic reduction of tumor cell-fraction (extent of tumor necrosis) accompanied by presence of a giant cell/histiocytic reaction, keratinous debris and fibrosis (Fig. 1C). pTR-1(10-49%) or pTR-2 (≥50%) was detected in surgical specimens from 15 patients (52%), similar to the overall pTR rate (44%) previously reported after a single dose of neoadjuvant pembrolizumab (3). Complete Pathologic Response (CPR) (pTR=100%) was observed in 1 tumor (3.4%) and Major Pathologic Response (MPR) (pTR>90%) was observed in 3 additional tumors (13.8% in total). Patient and disease characteristics did not differentiate responders (Rs, pTR-1 or -2) from non-responders (NRs, pTR-0), aside from the younger age (p=0.038) and enrichment of larynx/hypopharynx tumors (p=0.042) among non-responding patients (Table S4). RECIST CR/PR responses occurred in 5 (17.2%) tumors after neoadjuvant anti-PD-1, and pTR-1/-2 was enriched among these (p=0.016), with all 5 CR/PRs exhibiting pTR-2 (Fig. S1).

After two doses of neoadjuvant pembrolizumab and/or an extended treatment period (5 weeks versus 2-3), we observed a distribution of pTR categories weighted towards a higher rate of pTR-2 compared to previously reported pTR distribution after a single dose of pembrolizumab (45% vs. 22%, respectively; p=0.085 Fig. 1D) (3). The frequency of pTR-2 increased by 22.6% (95% CI: 0-45.2) compared to the single dose cohort (Table S5). We also observed a reduced rate of high-risk pathology, defined as presence of extranodal extension and/or positive margin in the surgically resected specimen (p=0.009, Table S5), which translated into a reduced need for adjuvant chemotherapy (p=0.043) after two doses vs. historical single dose neoadjuvant pembrolizumab.

TILs in HNSCC have profiles of cytotoxicity and exhaustion

To unravel the T cell dynamics associated with pTR after neoadjuvant PD1-blockade therapy, we profiled CD45+ CD3+ TILs (Fig. S2) isolated from 14 tumor biopsies collected either before or after PD-1 blockade through paired 5’ single cell transcriptome (scRNA-seq) and T-cell receptor sequencing (scTCR-seq). Samples were from 7 HNSCC patients treated with two doses of neoadjuvant anti-PD-1 (from cohort 2) and one-post therapy biopsy from a Cohort 1 patient who received one dose of anti-PD-1 (P36, Fig. 2A). The 8 patients comprised 4 Rs (achieving pTR-1 or -2) and 4 NRs (scored as pTR-0) following neoadjuvant anti-PD-1 therapy (Fig. 2A). Twelve of 14 biopsies collected from 6 patients (3 Rs [pTR= 60-70%, >90% and 100%, respectively] and 3 NRs) were matched pre- and post- 2-dose anti-PD-1 treatment specimens (cohort 2), separated by a median time interval of 35 days (range 33-42). After filtering T cells for expression of *CD8* transcripts (see Materials and Methods), we obtained 17,158 CD8+ TILs that could be assigned to 12

transcriptionally-defined clusters (Fig. 2B, Fig. S3A-B, Data File S1, S2). These clusters were classified based on RNA expression of T cell-related genes and by cross-labeling with reference gene-signatures from external single-cell datasets of human TILs (11, 13, 14) (Fig. S3C-E). The composite expression of genes associated with T cell memory, exhaustion, cytotoxicity or proliferation were used to devise scores related to these cell states that were then applied to characterize the identified cell clusters (see Materials and Methods). .

Upon examining these clusters further (Data File S2), we noted that most abundant terminally exhausted (T_{TE}) cell subpopulations could be clearly divided into 2 subsets. The first was characterized by extreme exhaustion ('T_{TE}-EEx') (Fig. 2C,D), whose most differentially expressed transcripts were related to an exhaustion program (i.e. *PDCD1, HAVCR2, TIGIT, CTLA4, TOX*) and associated with recognition of tumor antigens (*ENTPD1, CXCL13*) (14). The second 'T_{TE}-CTX' subpopulation, demonstrated characteristics of cytotoxicity (CTX: expressing *GZMH, GZMK, SLAMF7, EOMES*), and appeared less severely exhausted. While both subsets were characterized by high expression of markers of tissue residency (i.e. CD103 and CD49a integrins, encoded respectively by the genes *ITGAE* and *ITGA1*), they differentially expressed transcription factors, which likely reflected the activity of distinct gene expression programs. Indeed, T_{TE}-CTX exhibited the highest expression of cytotoxic molecules with striking expression of the *ZNF683* transcription factor, which has been associated with the maintenance of a tissue resident memory (TRM) program (15, 16) (Fig. 2C,D). Consistent with an effector-like activation, T_{TE}-CTX exhibited upregulation of HLA-class II genes. Conversely, the gene-program of T_{TE}-EEx was dominated by expression of *PRDM1* that, in conjunction with *TOX,* was associated with the highest level of exhaustion (Fig. 2C,D). This status was accompanied by increased expression of *TNFRSF4, TNFRSF9, ICOS* and *IL2RA*, all known to be acutely upregulated upon TCR stimulation (17, 18). Thus, the observed profile of extreme exhaustion suggested *in vivo* exposure to prolonged antigen stimulation.

To evaluate how the acquisition of the identified cell states could be affected by antigen recognition, we investigated the relationship between phenotype and TCR clonality in 4,716 distinct TCR clonotypes (see Materials and Methods) detected by scTCR-seq in 14,315 CD8+ TILs (Data File S1, Fig. S4A-B). As we previously observed in melanoma (14), CD8+ TCR clonotype families (i.e. T cells with identical TCRs) preferentially segregated into memory or exhausted states. Since these two T cell fates were generally mutually exclusive, we could classify most TCR clonotypes into one of two distinct states for downstream analysis of clonotype dynamics, wherein the "primary" phenotype was either 'Non-Exhausted Memory' (T_{NExM}) or 'Exhausted' (T_{Ex}) (Fig. 2B). The delineation of these two major states among TCR clones was supported by the high correlation between clusters within each of these transcriptionally-defined compartments (Fig. S4C). The acquisition of these two distinct phenotypes within the TME suggested the recognition of distinct antigen targets by these two groups of T cells (14, 19, 20). In support of this, T_{NExM} clusters were enriched in signatures of T cells with reported *in vitro*-verified specificity for viral antigens, while T_{Ex} clusters showed strong transcriptional similarities to the reported profiles of experimentally-confirmed tumor-reactive TILs (Fig. 2E) (14); these putative tumor-reactive cells largely resembled terminally differentiated TILs specific for tumor antigens, but also included low fractions of TILs enriched in progenitor exhausted signatures (14, 21, 22)

('T_{PE}-like'; Fig. S4D). Thus, our findings align with emerging evidence that interactions with tumor antigens shape the phenotype of TILs towards an exhaustion program (14, 20, 23).

Among $CD8^{neg}$ TILs, we identified 10 subpopulations enriched in *CD4* expression (Fig. S5A-C, Data File S3). The CD4+ TCR clonotypes segregated into 4 major transcriptionally-defined states (Fig. S5D,E): non-exhausted memory (T_{NExM}), exhausted (T_{Ex}), *GZMK*+ (T_{GZMK+}) and T regulatory (T_{Reg}) cells, each associated with activity of fate-specific transcriptional factors (*TCF7, TOX, EOMES* and *FOXP3*, respectively; Fig. S5C). As with the CD8+ TILs, we detected subpopulations of CD4+ T_{TE} cells with differing levels of cytotoxicity and exhaustion (Fig. S5B,C). T_{Ex} and T_{GZMK+} CD4+ TILs were enriched in signatures of CD4+ cells with *in vitro* validated tumor-specific TCRs (24) (Fig. S5F). CD4+ T_{Reg} TILs exhibited bimodal expression of activation markers (i.e. *TNFRFS4, TNFRFS9* and *TNFRFS18,* Fig. S5G,H) consistent with activated and non-activated T_{Reg} states (25). Overall, substantial fractions of CD8+ and CD4+ TCR clonotypes within the HNSCC TME had cell states characterized by moderate or extremely high expression of immune checkpoints and by evidence of cytotoxic potential, possibly resulting from stimulation by tumor antigens.

Distinct pre-treatment cell state profiles of HNSCC-TILs associated with response to PD-1 blockade

In our single dose pembrolizumab study, we showed CD8+ T cell infiltration associated with pTR (3). In the current study, scRNA-seq analysis provided a higher resolution analysis of this association. Notably, the pretreatment TME of Rs was composed of higher frequencies of CD8+ T_{Ex}-TILs compared to NRs ($p<0.0001$, Fig. 3A), most of which were attributable to the T_{TE}-CTX subpopulation (13.4-fold difference, $p=0.0102$, Fig. 3B, Data File S4). Likewise, phenotypic classification of CD8+ TILs collected before neoadjuvant immunotherapy revealed an elevated frequency of T_{TE}-CTX TILs in 1 of 6 independent HNSCC patients previously profiled by scRNA-seq (12) with this patient having the most striking pathologic response of the group (pTR-2, Fig. S6A). Compared to NRs, pre-treatment CD8+T_{Ex} cells from Rs were enriched for the expression of cytotoxicity genes (*PRF-1, IFNG, GZMA, GZMB, GZMH, GNLY*), markers of effector-like activation (e.g. upregulation of HLA-class II transcripts) and genes associated with maintenance of a TRM-program (15) (*ZNF683*+) (Fig. 3C, Data File S5). This profile of high functionality of the CD8+T_{Ex} cells from Rs was further supported by the observed enrichment of previously reported gene signatures associated with high effector function (i.e. elevated IFN response, TCR signaling) (10, 26, 27) (Fig. 3D). Multiplex immunofluorescence (IF) of pre-treatment biopsies in 17 patients treated with 2 doses of pembrolizumab (cohort 2) confirmed that Rs (compared to NRs) were more highly infiltrated with CD3+ CD8+ TILs (Fig 3E, 3F-**top** $p=0.0274$), and that these cells co-expressed PD-1 and the integrin CD103, a well-established surface marker profile for identification of TILs with TRM phenotype (28, 29) (Fig 3E, 3F-**bottom** pval=0.0592, Fig. S6B, Data File S6).

Among baseline CD4+ TILs, we observed a similar enrichment of exhausted cells in R patients ($p=0.0122$, Fig. S7A,B, Data File S4). In NRs, this was counterbalanced by higher

frequencies of CD4+ T_{NExM}. While the proportion of T_{Reg}-TILs between the two groups of patients was similar, the low abundance of putative tumor-reactive CD8+ T_{Ex} in NRs resulted in a relatively higher proportion of CD4+T_{Regs} per exhausted CD8+ TIL, consistent with a more immunosuppressed TME (Fig. S7C). As for CD8+ TILs, pretreatment CD4+ T_{Ex} TILs from Rs were enriched for genes related to cytotoxicity, effector-like activation and a TRM-program (*ITGAE,* encoding for CD103) (Fig. S7D). Altogether, CD8+ and CD4+ T cells infiltrating HNSCC lesions at baseline were quantitatively and qualitatively distinct in patients responsive to neoadjuvant anti-PD-1 immunotherapy. In particular, responders exhibited high numbers of putative anti-tumor CD8+ T_{Ex} TILs in a TRM-like state and with high cytotoxic potential.

Dynamics of TIL cell states following neoadjuvant anti-PD-1

To evaluate the impact of PD-1 blockade on the global phenotype of CD8+ and CD4+ TILs, we compared TILs from the 6 paired sets of pre-post biopsies. Five weeks after immune checkpoint blockade initiation, the 3 Rs consistently demonstrated relative contraction of the CD8+ T_{Ex} compartment (p=0.0181), counterbalanced by an increase in CD8+ T_{NExM} cells (p=0.0008; Fig. 4A, Data File S4); a moderate reduction of CD4+ T_{Ex} and T_{Reg} cells frequencies (p=0.0383 and p=0.0389, respectively) and an increase in CD4+ T_{GZMK+} cells (p=0.0383) among CD4+ TILs (Fig. S8A). In contrast, the relative proportions of CD8+ and CD4+ phenotypes were not affected by PD-1 blockade in the 3 NRs, or showed opposite behaviors compared to Rs (e.g. CD4+ T_{Regs} enriched in non-responding lesions, p=0.0381). Following therapy, the global profile of CD8+ T_{Ex}-TILs was characterized by reduced expression of genes of cytotoxicity and of TRM (*GZMA, IFNG, ZNF683*; Fig. 4B). In line with this, most of the relative contraction within the T_{Ex} compartment of responding lesions originated from reduction of CD8+ T_{TE}-CTX TILs (p=0.0095, Fig. 4C, Data File S4). Hence, the same populations highly enriched in R-TILs at baseline were the most impacted by PD-1 blockade, supporting the primary role of T_{TE}-CTX in sustaining productive pTRs. In contrast, putative tumor-reactive CD8+ T_{Ex}-cells infiltrating non-responding lesions maintained their state of severe exhaustion, and demonstrated an increased proliferation score, consistent with accumulation of T_{TE}-EEx within the post-therapy TME (Fig. 4B-C).

As confirmation of these findings, we analyzed baseline gene-signatures predictive of response or non-response (Data File S5) in the post-therapy TILs. Using transcriptional comparisons between Rs and NRs CD8+T_{Ex}-TILs at baseline, we created signatures (adj_pval<0.01, $\log_2$FC>1, Data File S5) of response (49 genes, 'R-Pre-T_{Ex}') and non-response (123 genes 'NR-Pre-T_{Ex}'). Indeed, even after PD-1 blockade, the profiles of T_{EX}-TILs collected from Rs and NRs remained largely distinct and maintained enrichment of those gene signatures identified at baseline (Fig. 4D). Even CD4+ T_{Reg}-TILs detected in post-treatment biopsies from NRs retained a high level of activity, as evidenced by maintenance of an active proliferative state and enrichment of a gene-signature of activated T_{Regs} (Fig. S8B-D). Responders, instead, experienced a reduction of T_{Reg}-Act TILs after PD-1 blockade (p=0.0051, Fig. S8B, Data File S4), with the associated loss of activation signatures within T_{Regs} (Fig. S8C,D), which we speculate would contribute to a less immunosuppressive TME.

Consistent with the notion that treatment outcomes seemed to largely depend on the pre-existing status of the intratumoral T cell compartment, Rs had a higher fraction of CD8+ T_{Ex}-TILs with elevated cytotoxic potential prior to treatment administration (Fig. 5A, Data File S4). This qualitative difference was associated with a substantial quantitative increase of TRM-like CD103+ PD-1+ CD8+ T cells infiltrating pre-treatment HNSCC biopsies of Rs compared to NRs (p=0.0186, Fig 5B), especially in patients who experienced stronger responses (pTR-2 vs pTR-0: p=0.0089, Fig 5B) after treatment with 1 or 2 doses of neoadjuvant anti-PD-1 (cohorts 1 and 2, respectively), as assessed with IF (Data File S6). The intratumoral density of TRM-like CD8+ TILs increased slightly after neoadjuvant therapy but remained higher in Rs compared to NRs even at post-therapy timepoints (p=0.0464, Fig. 5C, Data File S6), documenting that relative contraction of T_{TE}-CTX did not impact the absolute number of CD8+ T cells infiltrating HNSCC lesions after therapy.

In line with these observations and as independent validation, analysis of baseline bulk RNA-seq in 26 patients from our previously reported single dose neoadjuvant anti-PD-1 clinical trial (3) confirmed more CD8+ infiltration in Rs vs NRs (p=0.0342, Fig. 5D-**top,** Data File S7). From this separate cohort, the baseline expression of *ZNF683* and cytotoxicity (CTX) genes (characteristic of T_{TE}-CTX) was enriched in patients with pTR1-2 (p=0.0014, Fig. 5D-**bottom**). Analysis of an external dataset with available bulk tumor RNA-seq data from 11 patients treated with 3 doses of neoadjuvant nivolumab (30) further confirmed that the *ZNF683*+ *CTX*+ signature was enriched in patients with a high degree of response (p=0.0357, Fig. 5E, Supplementary Methods). Such differences were not observed in the post-treatment samples (Fig. 5D-E, Data File S7). Together, these studies point to the support of high pathological responses (pTR-2) by high levels of pre-existing exhausted/cytotoxic TILs whose frequencies exhibit dynamic changes within the CD8+ T cell compartment paralleling elimination of cognate tumor antigens. We infer that these responding TILs constitute the major source of antitumor cytotoxicity following anti-PD-1 treatment, resulting in pTR. In turn, we reason that in the absence of this population (as in NRs with pTR<10%), PD-1 blockade was unable to reverse the severe dysfunction of CD8+ T_{Ex}-EEx TILs in the TME of NRs.

TCR clonotype dynamics associate with response to PD-1 blockade

Using scTCR-seq analysis, we then evaluated the dynamics of individual intra-tumoral TCR clonotypes in relationship to the T_{NexM} or T_{Ex} phenotypes in matched pre-post therapy biopsies. These findings revealed qualitative differences in the expanded specificities in the two response groups: Rs displayed a majority of pre-treatment CD8+ T_{Ex}-TILs with highly expanded clonotypes with a predominant T_{TE}-CTX phenotype and NRs had considerably fewer expanded CD8+ T_{Ex}-TCR clonotypes, which preferentially exhibited a T_{TE}-EEx phenotype (Fig. 6A,B). By comparison, the predominant T_{EM} phenotypes of CD8+ T_{NexM}-TCRs were similar across all the patients (Fig. 6B). The analysis of dominant clonotypes among CD4+ TILs was limited by their lower level of clonal expansion within the TME. Nonetheless, Rs still demonstrated dominant CD4+ T_{Ex} clonotypes at baseline (Fig. S9A), and the phenotypic distribution of dominant CD4+ clones within each compartment was not perturbed by therapy (Fig. S9B). Altogether, effective response to neoadjuvant

immunotherapy was characterized by the presence at pre-therapy of expanded and exhausted T cell specificities with cytotoxic potential.

Previous studies have shown that in response to anti-PD-1, influx of new clonotypes ('clonal replacement') represents a key fraction of post-treatment intra-tumoral T cells (11). To examine the persistence of pre-existing TCR clonotypes or the intra-tumoral influx of T cells with novel specificities, we categorized TCR clonotypes as: i) only detectable in pre-therapy ('*lost*'), ii) only present post-therapy ('*new*'), or iii) observable in both pre- and post-therapy timepoints ('*persisting*', Data File S8). Numerous novel TCR clonotypes emerged among post-therapy CD8+ and CD4+ TILs (Fig. 6C, Fig. S10A), but most were not expanded (i.e. were detected in the sequencing data only as singletons; Fig. 6D, Fig. S10B). Thus, *'new' expanded* clones (>2 cells) contributed minimally to the post-treatment anti-tumor T cell repertoire of both Rs and NRs. Moreover, the majority of these novel specificities could have arisen as a result of sampling bias rather than active recruitment of novel tumor-reactive clones within the tumor (i.e. "clonal replacement"(11)) – at least within the short one month timeframe following neoadjuvant PD-1 blockade. In contrast, numerous clonotypes detected at baseline *persisted* after anti-PD1 therapy, accounting for ~60-70% of CD8+ TILs and ~15-40% of CD4+ TILs in both pre and post-treatment biopsies, with Rs demonstrating a larger fraction of persisting CD8+ or CD4+ clones originating from pre-treatment timepoints (pre-existing) compared to NRs ($p=0.0414$ and $p=0.0234$, respectively, Fig. 6C, Fig. S10A). Similar dynamics of T cell clones were observed in an independent cohort of 6 HNSCC patients (3Rs and 3NRs) who received pre-surgical administration of 3 doses of nivolumab (30) (Fig. S10C-D): persisting clones identified in both pre- and post-therapy tumor biopsies through bulk targeted TCR-beta chain-seq constituted the largest fraction of TILs. In both internal and external cohorts, these persisting T cell clones were also more expanded, especially in the baseline biopsies from Rs (Fig. 6D, Fig. S10B-D). Our ability to profile the cellular state of TCR clonotype families allowed further investigation of the dynamics of clones with distinct phenotypes: after anti-PD-1 therapy, persisting and expanded CD8+ T_{Ex} clones specifically contracted in Rs after treatment ($p=0.0152$; Fig. 6E, F). In line with such relative shrinkage, Rs displayed a high fraction of expanded CD8+ T_{Ex} clones that were lost following treatment ($p=0.0043$, Fig. 6E, Data File S9), while NRs lacked evidence of T_{Ex} clonal dynamics. Although the size of persisting CD8+ T_{NexM}-clones increased in both Rs and NRs ($p<0.0001$, Fig. 6F-**top**), only the dynamics of CD8+ T_{Ex}-TCR clonotypes differed between the two patient groups ($p<0.0001$, Fig. 6F-**bottom**), thus highlighting putative-tumor reactive pre-existing CD8+ T_{Ex} clones as major determinants of effective response after PD-1 blockade. In Rs, we further observed a moderate expansion of persisting CD4+ TCR-clonotypes with a T_{GZMK+} phenotype following anti-PD-1 treatment (Fig. S11A,B).

Maintenance of persisting TCR clone phenotypes underscores the impact of pre-existing ZNF683+ CTX+ T_{EX} clonotypes in treatment response

As response to neoadjuvant anti-PD-1 correlated with contraction of T_{EX} clonotypes, we next asked if these changes impacted the phenotypic quality of T cell clones sustaining the productive pTRs. We found that *persisting* TCR clonotypes of both CD8+ and CD4+ TILs maintained a distribution among the various cell states that was not dissimilar to

that observed at baseline (Fig. S12A,B). Indeed, 180 (95%) of the 189 *persisting* CD8+ clonotypes classified as T_{NexM} or T_{Ex} and detected as expanded (>2 cells) at baseline maintained their original primary phenotype in the post-treatment biopsies. We did not find any evidence of significantly altered pathways in T cell function in a comparison of the transcriptional profiles of pre and post therapy single cells with persisting T_{Ex} TCRs. These observations support the notion that anti-PD-1 therapy in HNSCC is unlikely to reshape the fate of different T cell states within one month.

As the primary phenotypes were not altered after therapy, we then focused on genes defined in T cell signatures of response or non-response to immunotherapy (Data File S5). Amongst all the *lost*, *new* or *persisting* T_{NexM} or T_{Ex}-TCR clonotypes (Fig. 7A-**left**), we found that the putative-tumor reactive T_{Ex} TCR-clonotypes exhibited most of the differences associated with response to therapy. Among the CD8+ T_{Ex}-clones, the highest levels of transcripts associated with response ('R-Pre-T_{Ex}' and 'cytotoxicity' genes) were expressed by *persisting* or *lost* TCR clonotypes detected in Rs at baseline (pre). Among expanded clonotypes in Responders, the same T cells had the highest cytotoxicity score and moderate levels of exhaustion (Fig. 7A-**right**). By contrast, *persisting* CD8+ T_{Ex} clones of NRs at both pre and post timepoints were highly enriched for features associated with lack of response ('NR-Pre-T_{Ex}' and 'exhaustion' genes, Fig. 7A-**left**) and expanded clones from these patients exhibited the most elevated levels of exhaustion, which remained unchanged after PD-1 blockade (Fig. 7A-**right**). Increase in expression of proliferation genes was not observed in Rs, but was associated with lack of response, as observed in *persisting* or *new* CD8+ T_{Ex} clones in NRs. Finally, no evident significant differences between *lost/new/persisting* CD8+ clones with a T_{NexM} phenotype were associated with response to anti-PD-1 therapy. In line with these results, the level of exhaustion among putative tumor-reactive CD8+ T_{Ex}-TCR clonotypes did not diminish nor did they acquire memory properties, whether from Rs or NRs (Fig. 7B,C, Data File S9). Moreover, Rs did not experience post-therapy accumulation of non-exhausted CXCL13+ CD8+ TILs (Fig. S13A), which has been observed in other clinical settings as a consequence of the reinvigoration of antitumor responses (10). Therefore, in HNSCC, the conversion of T cell clones towards less-exhausted phenotypes was infrequent, at least within the relatively short 1-month timeframe of sample collections.

Overall, these data point to the cellular quality of expanded *persisting* or *lost* CD8+ T_{Ex}-TCR clonotypes detected at baseline as a major factor associated with response, thus linking the success of neoadjuvant anti-PD-1 therapy to pre-existing CD8+ TCR clonotypes with high cytotoxic potential and a TRM program (*ZNF683*+CTX+) within the HNSCC microenvironment. Upon tracking the dynamics of this population of T cells, we observed them to constitute an average of 55% (range 39-69%) of CD8+ T_{Ex}-TCRs in baseline R TILs (Fig. 7D,E-**top,** Data File S9) and an average of 32% (range 22-40%) of total CD8+ TILs (Fig. 7F-**top**, Fig. S13B). Concomitant expression of *ZNF683* and CTX-genes was exhibited by highly expanded clones and was specific for T_{Ex}-TCRs rather than T_{NexM}-TCRs (Fig. 7D,E, Data File S9). In NRs, such populations were dramatically underrepresented (p=0.0073, Fig. 7F-**top**, Fig. S13B, Data File S9) with only a mean of 4% (range 1-8%) of total CD8+ TILs. After PD-1 blockade, *ZNF683*+ CTX+ T cells

exhibited the most profound change associated with response within HNSCC CD8+ TILs, thus supporting their central role in immune reactions underlying effective responses (Fig. 7D,E). The 5-fold decline of these cells in Rs (p=0.0104, Fig. 7F-**top**) was mainly explained by the loss or contraction of expanded T_{Ex} clones (p=0.0057, Fig. 7F-**bottom**). In contrast, tumors with poor pTR were associated with pre-existing CD8+ T_{Ex} TCR-clonotypes in a state of severe exhaustion rather than a ZNF683+ CTX+ state (Fig. 7A), a condition that could not be reversed, resulting in accumulation of exhausted clones in non-responding HNSCC lesions.

To assess if the population we identified in this study could also be associated with therapeutic response outside of HNSCC, we quantified the *ZNF683*+ CTX+ CD8 TILs in the TME of other cancer types using publicly available external scRNA-seq datasets of TILs collected before and after immune-checkpoint therapy (10, 11, 31). For patients with BCC, cSCC or melanoma, *ZNF683*+ CTX+ T cells were not highly abundant in CD8+ TILs, and the frequencies of this population did not differ by clinical outcomes or timing in relationship to immunotherapy treatment (Fig. S13C-E). Higher proportions of *ZNF683*+ CTX+ T cells were detected in NSCLC Rs (Fig. S13F), although only 2 of 8 responsive patients showed frequencies comparable to those observed in HNSCC Rs (>20%). In line with our current study, these 2 NSCLC patients similarly demonstrated a contraction of *ZNF683*+ CTX+ T cells upon response to immunotherapy. Thus, we observed that in these PD-1 blockade responsive HNSCC patients, pre-existing T cells with cytotoxicity potential were present at the highest frequencies when compared with the solid tumor malignancies that we evaluated.

Discussion

Defining the fate and trajectory of critical T cell populations in the face of exposure to active immunomodulatory agents such as PD-1 blocking antibodies provides an opportunity to gain mechanistic understanding of the basis of response to such therapies. Neoadjuvant anti-PD-1 therapy has been shown to be active across several types of malignancies, including HNSCC, but mechanisms underlying responses are only beginning to be defined. Clinical observations from the current phase II trial testing two-dose neoadjuvant anti-PD-1 for HNSCC included a trend towards an increase in pTR-2 frequency and a reduced frequency of high-risk pathology following surgery compared to our previously reported single neoadjuvant dose trial (3). Through single cell transcriptome and T cell clonotype tracking analysis of paired pre- and post-treatment HNSCC tumor specimens, we gained insights into the T cell dynamics of TILs at a defined ~5 weeks following a first neoadjuvant anti-PD-1 dose. Revival of pre-existing specificities into less exhausted phenotypes was not observed, while the recruitment of novel and expanded clones was minimal early after immunotherapy. Rather, we discerned Rs at baseline to display an elevated population of pre-existing intra-tumoral exhausted *ZNF683*+ T cells with high cytotoxicity potential and subsequent relative contraction of this subpopulation in concert with tumor regression, implicating “cytotoxic revival” (Fig. S14). Therefore, this phenomenon is not based on reinvigoration of a phenotype, but rather, on reinvigoration of function. Our data indicate that PD-1 blockade leads to the unleashing of the cytotoxic potential of TRM-TILs when

they are not surgically removed in advance of immune checkpoint blockade therapy, thus leading to a rapid first line of response after therapy administration.

Although we were unable to experimentally measure cytotoxic activity of the ongoing clinically evident immune response, several lines of evidence convincingly pointed us towards this mechanism. First, functional revival would require the existence of expanded clones with cytotoxic potential already at baseline (T_{TE}-CTX), which we verified to be the case for HNSCC Rs, while the expanded clonotypes of NRs at baseline had signatures of extremely high exhaustion (T_{TE}-EEx). We posit that the severe exhaustion observed in NRs likely eroded the baseline T_{TE}-CTX compartment leading to a lack of anti-PD-1-induced pTR. Second, the notion of revival of the functional cytotoxicity of these dominant clones would suggest that their potential for cytotoxicity was rendered latent prior to PD-1 exposure due to concurrent immune inhibition (e.g. PD-1 expression). Indeed, we found these exact features present in putative tumor-reactive T_{TE}-CTX TIL clones of Rs. Third, such cytotoxic T cell subpopulations would be expected to persist over the course of therapy, exhibit the most dynamic change following neoadjuvant PD-1 therapy and drive pathological response to neoadjuvant PD-1 blockade. In fact, we observed such clonal trajectories for putative tumor-reactive T_{Ex}-TILs in patients who experienced pTR, but not for NRs. Importantly, the primary phenotypes of a high number of *persisting* clonotypes were generally stably maintained across time despite therapy, making clonal revival unlikely. Our profiling thus reveals the fundamental pre-existing biologic differences in the landscape of baseline TILs and their capacity to respond to anti-PD-1 antibody-mediated disruption of immune inhibitory signals, and in turn, to impact the ability of individual patients to raise effective anti-PD-1 induced anti-tumor responses.

Rs and NRs could not be distinguished based on extent of newly expanded memory clonotypes. However, a key feature of the observed T cell clonal dynamics was the relative contraction of the pre-existing T_{TE}-CTX population in patients with high pathological responses (pTR-2). While such dynamics might appear counterintuitive with respect to a neoadjuvant anti-PD-1-induced pTR, it mirrors the kinetics of diminishing availability of cognate tumor antigens in the setting of tumor eradication (Fig. S14). Our data implicating the dependence on antigen-specific stimulation for the persistence of T_{TE}-CTX clones are consistent with recent data on requirement of antigen to maintain tumor-specific TRMs (32) and not due to a reliance on propagation from memory progenitor cells as has been described for other tumors (10). The relative contraction of T_{TE}-CTX in Rs might derive also from the alteration of the tumor architecture following a productive antitumor response, which can cause tumor necrosis and consequent destruction of immune niches. Conversely, for NRs, the lack of dynamics in T_{TE}-EEx and the absence of clonal revival led us to speculate that anti-PD1 treatment in these patients is unable to reprogram antitumor TILs, at least within the one-month perioperative period. Several factors could contribute to the decrease of T_{TE}-CTX in favor of T_{TE}-EEx in NRs: although speculative, as observed in other cancer types, interactions with tumor cells expressing high amounts of immune checkpoint ligands or with abundant immunosuppressive myeloid populations could exacerbate the exhaustion of putative tumor-reactive TILs (33, 34); this could be further aggravated by the lack of intratumoral tertiary lymphoid structures or extratumoral secondary lymphoid tissues that are able to sustain the persistence of less exhausted effectors

(35). Finally, it is unknown whether the quality and quantity of tumor antigens recognized by TILs greatly differ between Rs and NRs and how they impact on the differentiation of antitumor TILs. Indeed, in other contexts, the presence of strong tumor antigens such as viral oncoproteins in HPV+ HNSCC has been associated with improved response to immunotherapy (36), as a result of the presence of high amount of virus-specific CD8+ TILs encompassing different degrees of exhaustion (21). Future studies will be required to assess which of these mechanisms is predominant within the TME of HNSCC.

While we found support for “cytotoxic revival” in HNSCC, we also found evidence of this mechanism of anti-PD-1 response in NSCLC, where certain responder patients were found to have a *ZNF683*+ CTX+ population at baseline. Our work thus supports the notion that the cytotoxic effector CD8+ TILs with a TRM-program (15, 16, 37) (*ZNF683*+CTX+) have a pivotal role in sustaining effective antitumor immunity within the TME and are major players in determining response to immune checkpoint blockade (38, 39). In line with this, different groups have shown that the presence of elevated CD8+ TILs with TRM-features is associated with positive outcomes after immunotherapy (29, 38, 40-43), thus highlighting the importance of such populations both as a predictive biomarker and as a reservoir of antitumor specificities that can be unleashed after PD-1 blockade. The role of pre-existing *ZNF683*+CTX+ TILs might be pivotal in the clinical setting of neoadjuvant immunotherapy, where intratumoral TILs are not surgically removed before therapy and consequently can provide a rapid antitumor response following their reinvigoration. We speculate that the mechanism of cytotoxic revival might be favored in the short window following neoadjuvant approaches and may thus be active only in patients that already have a large population of exhausted infiltrating T cells with a cytotoxic signature, as seen in HNSCC or NSCLC. In other clinical settings, where *ZNF683*+CTX+ TILs are low in frequency or are largely surgically removed before immunotherapy, other mechanisms sustained by T cells from extratumoral sites (lymph nodes or peripheral tissues) might be favored, as has been found at later timepoints (2-3 months) in BCC and cSCC treated with adjuvant immunotherapy (11). The lack of clonal revival early after neoadjuvant anti-PD-1 might derive from the quantitative and qualitative differences observed in HPV-negative HNSCC lesions among progenitor exhausted TILs, which in other cancer types have been reported to sustain the accumulation of non-exhausted putative tumor-reactive TILs (10). Furthermore, we note that recent HNSCC studies show that response to neoadjuvant anti-PD-1/CTLA-4 includes clonal replacement from the systemic circulation compared to anti-PD-1 monotherapy alone (12) suggesting that the specific therapeutic context can dictate clonal dynamics. Thus, our findings point to the different and preferential modes by which PD-1 therapy may be active depending on the disease type, the therapeutic context, the treatment schedule and the time of analysis. Indeed, we cannot exclude that mechanisms such as clonal revival or replacement may be operative even for HNSCC outside of the neoadjuvant window, since phenotypic conversion of existing clones or recruitment of new specificities might require longer times of action. As demonstrated by other groups (10, 11), the role of extra-tumoral specificities and T_{PE}-like populations might be preponderant 2-3 months after treatment initiation, and in clinical setting where intratumoral T_{TE}-CTX are removed with the surgery.

Our study has multiple translational implications. From the clinical standpoint, our previously reported single dose neoadjuvant PD-1 study with extension to the current two

dose study are the first in HNSCC to examine distinct anti-PD-1 dosing approaches. The present two-dose trial demonstrated excellent safety and tolerability in the peri-operative window. Interestingly, we noted that although the total fraction of Rs (pTR-1 or -2) in single dose and two dose cohorts were similar, we observed a shift to more patients manifesting pTR-2 with two doses of anti-PD-1 therapy. These data suggest that two doses and an extended dosing period was unable to convert NR patients to Rs. Differences in study populations and the modest number of enrolled subjects caution against any overinterpretation. Although neoadjuvant anti-PD-1-induced partial pTR was associated with better HNSCC clinical outcomes (4), validation in a controlled clinical trial is necessary. As further immunotherapies are tested within the neoadjuvant paradigm, attention to timing and dosing of these agents will likely be critical to obtain optimal tumor pathologic responses. From a response-prediction standpoint, the identification of quantitative and qualitative differences within the baseline TME of Rs and NRs allowed delineation of metrics that are associated with strong responses to neoadjuvant immunotherapy: as we verified in internal and external cohorts, high frequencies of putative tumor-reactive T_{TE}-CTX in baseline Responders lesions are paralleled by an enrichment of *ZNF683*+ CTX+ signature in bulk tumor RNA, and translate to high numbers of TRM-TILs. Therefore, quantification of such parameters on pre-treatment lesions through bulk tumor RNA-seq or through multiplexed immunofluorescence could be exploited to stratify patients. Of note, these metrics do not allow stringent differentiation between T_{TE}-CTX and T_{TE}-EEx, which are currently reliably quantified only through scRNA-seq, but rather provide an indirect measurement of the increase in T_{TE}-CTX. Therefore, further application of these proposed metrics to other HNSCC cohorts will be necessary to fully develop their predictive power in this tumor context. Future studies that provide further elucidation of the similarities and differences of the HNSCC TME compared to other tumors are anticipated to enable the translation of single cell-based signatures of tissue resident CD8+ T cells into a clinically actionable biomarker.

Materials and Methods:

Study Design

The main objective of the study was to evaluate pathological tumor response in HNSCC patients treated with two doses of neoadjuvant pembrolizumab (“cohort 2”) and to investigate T cell dynamics associated with responses to pre-surgical immunotherapy. Response to neoadjuvant anti-PD1 was defined as pathological tumor response (pTR), quantified at surgery based on histologic reduction of tumor cell-fraction and extent of tumor necrosis (Fig. 1A). In selected patients with available material, dynamics of TILs were investigated through scRNA-seq of FACS sorted CD3+ CD45+ tumor fractions (Fig. 2A, Fig. S2). This allowed identification of increased of TEx-TILs in baseline HNSCC tumors from Responders, which was extended through quantification of PD-1+ CD103+ CD8+ TILs using immunofluorescence staining of primary tumors (Fig. 3E-F). The same immunofluorescence analysis was extended to pre-treatment biopsies collected from patients treated with one dose of neoadjuvant pembrolizumab (cohort 1). We used transcriptomic data available from cohort 1 (3) and from an external dataset (30) to demonstrate the enrichment of CD8+ TILs and ZNF683+ CTX+ gene signature in HNSCC tumors from

pre-treatment biopsies (Fig. 5). Finally, we exploited scTCR-seq of pre-post therapy TILs in conjunction with scRNA-seq to describe the behavior of T cell clones with exhausted or memory phenotype; this allowed us to investigate the dynamics and phenotypes of TCR clonotypes associated with pTR (Fig. 6-7).

Clinical trial design

Between February 8, 2018, and December 3, 2020, 29 patients with resectable clinical stage III-IVb (normalized to AJCC 8th Edition) HNSCC enrolled into group 2 (referred to as Cohort 2) of a multicenter, phase II clinical trial (NCT02296684), approved by the Institutional Review Boards (IRB) of Dana-Farber/Harvard Cancer Center (DFCI#16-385), Washington University (#201412118) and Memorial Sloan-Kettering Cancer Center (MSKCC) (#18-379). The trial protocol is available as Supplementary Materials. Enrolled patients had pathologically confirmed diagnosis of HPV-unrelated (oral cavity, hypopharynx, larynx or p16-negative oropharynx) HNSCC, measurable disease per Response Evaluation Criteria in Solid Tumors (RECIST)v1.1, Eastern Cooperative Oncology Group (ECOG) performance status 0-1, and adequate marrow and organ function (absolute neutrophil count >1,500/mcL, platelets >100,000/mcL, hemoglobin >9g/dL; total bilirubin <1.5x upper limits of normal [ULN], AST and ALT <2.5x ULN; serum creatinine <1.5x ULN or creatinine clearance >30 mL/min).

Key exclusion criteria included HPV-related oropharynx SCC, active autoimmune disease, or immunodeficiency. Tests required to determine eligibility included complete blood count, metabolic panel, pregnancy test (women), coagulation and thyroid panels, urinalysis, and CT scans of the neck and chest. This study was conducted in accordance with the Declaration of Helsinki.

Procedures

Cohort 2 patients received two doses of neoadjuvant pembrolizumab (each 200 mg, IV, q3 weeks) beginning 33 to 50 days prior to surgical resection with curative intent. Baseline and post-neoadjuvant pembrolizumab CT scans were performed for 29 patients as previously described (3). Tumor volumetric response was assessed using modified RECISTv1.1, as restaging scans were not repeated due to surgical resection. Surgery included resection of all gross disease at the primary site. Therapeutic/prophylactic neck dissection and reconstruction were performed as appropriate. Surgery was performed according to the initial planned resection margins and was not modified by neoadjuvant treatment response. Adjuvant therapy for Cohort 2 patients was not dictated by the trial protocol, and adjuvant treatment including radiation therapy or cisplatin-radiation therapy was based on disease risk features and consistent with standard of care. Tumor samples were obtained at baseline, prior to neoadjuvant therapy, and at surgery, and processed for single-cell analyses. Due to sample requirements of scRNASeq, we were limited to collecting tissues from the 8 patients accrued at the Dana-Farber Cancer Institute. Specimens were collected and analyzed under the auspices of DFCI IRB-approved protocol #18-092. The primary endpoint was rate of pathologic response present in the surgically resected cancer of ≥50% (pTR-2). Pathologic response was independently assessed in the surgical resection specimens by two head and neck pathologists with consensus review of discrepant cases. Primary tumor and lymph

node disease were graded separately, and pTR assigned based on the greater response as previously reported(3).

Adverse events were assessed within 30 days of last neoadjuvant pembrolizumab dose using CTCAE version 4.0. Events of Clinical Interest included elevated AST, ALT, bilirubin or alkaline phosphatase that occurred from the date of first dose through 90 days following the last dose of neoadjuvant pembrolizumab. Peri-surgical AEs were assess using Clavien-Dindo Classification of Surgical Complications (44).

ScRNA-seq and scTCR-seq analyses were conducted on 8 patients with stage III/IV HNSCC (Fig. 2A). In selected experiments (Fig. 1, Fig. 5D,E), the analysis was extended to an independent cohort of HNSCC patients (referred as cohort 1) treated with one dose of neoadjuvant anti-PD-1, as previously reported (3). The updated clinical data of such patients are summarized in Table S5. All patients provided written informed consent for the collection of tissue samples for research and genomic profiling.

Processing of tumor biopsies for single-cell sequencing

Fresh tumors collected from biopsies were mechanically and enzymatically disaggregated in dissociation buffer consisting of RPMI (Life Technologies) +10% FBS (HyClone), 100 U/ml collagenase type IV (Life Technologies), and 50 μg/ml DNase I (Roche). Suspension cells were incubated at 37°C for 45 minutes and then further mechanically dissociated. Red blood cells were removed from samples using red blood cell lysis buffer (Biolegend). Samples were pelleted and then resuspended in fresh RPMI +10% FBS and strained through a 40μm filter. Cells were incubated with the Live/Dead Zombie Green (Biolegend, cat# 423111) for 5 min in the dark at room temperature. Fc receptors were blocked prior to surface antibody staining using Human TruStain FcX Blocking Reagent (Biolegend). Cells were stained for 15 min on ice in the dark using antibodies specific for human CD45 (PE-conjugated, clone HI30, Biolegend, cat# 304008, 1:50) and human CD3 (PE-Cy7 conjugated, clone SK7, Biolegend, cat# 344815, 1:50). Samples were washed 2 times and sorted using a BD FACS Melody instrument, to isolate viable (Zombie-neg) CD45+ CD3+ lymphocytes. A representative sorting-strategy is reported as Fig. S2. Sample processing for single-cell gene expression (scRNA-seq) and TCR V(D)J clonotypes (scTCR-seq) was performed with Chromium Single Cell 5′ Library and Gel Bead Kit (10x Genomics), following the manufacturer's recommendations (Supplementary Methods).

Processing of single-cell data

Processing of scTCR data.—TCR-seq data for each sample were were aligned to the human hg38 reference genome and RefSeq gene models using Cell Ranger vdj (version 3.0.2) (https://www.10xgenomics.com/). TCRs were grouped in patient-specific TCR clonotype families based on TCRα-TCRβ chain identity, allowing for a single amino acid substitution within the TCRα-TCRβ CDR3. Cells with a single TCR chain were included and grouped with the matched clonotypes families. The resulting TCR clonotype families were ranked according to sample-specific size and incorporated into downstream analysis. Samples from the same patient were combined, TCR clonotype grouping was reiterated for each patient and results were manually reviewed. Based on detection in

pre-post tumor biopsies, each TCR clonotype was further classified as “Lost” (detected only in pre-therapy timepoint), “New” (detected only in post-therapy timepoint) or Persisting (detected in both timepoints). TCR clonotype families were considered “expanded” when composed by at least 3 T cells in a single timepoint.

Processing and analysis of scRNA-seq.—scRNA-seq data were processed with Cell Ranger software (version 3.0.2). Filtered gene-barcode matrix files containing gene counts matrices were read into Seurat (version 4.1.0)(45). Cells were filtered to retain those with ≤20% mitochondrial RNA content and with a number of unique molecular identifiers (UMIs) comprised between 250 and 10,000. Overall, scRNA-seq data comprised 150,795,226 transcripts in 42,009 cells that passed quality filters. scTCR data were integrated and cells with ≥3 TCRα chains, ≥3 TCRβ chains or 2 TCRα and 2 TCRβ chains were removed. scRNA-seq data was normalized using Seurat NormalizeData function. Cells from different experimental batches were combined using the RunHarmony function in Seurat with default parameters (46). CD8+ and CD8- (CD4+) TILs were identified and clustered as reported in Supplementary Methods. For both CD8+ and CD8- objects, cluster classification was performed using RNA expression of a panel of T cell-related genes and by cross-labelling with reference gene-signatures from external single-cell datasets of human TILs (11, 13, 14). We assigned to each cells scores that summarized important T-cell related features. We used Seurat’s function AddModuleScore with default parameters to analyze expression of representative T-cell genes and to determine the following scores: memory score (*IL7R, SELL, CCR7, CD28, TCF7*), exhaustion score (*PDCD1, HAVCR2, TIGIT, CTLA4, LAG3, TOX*), proliferation score (*MKI67, TOP2A, STMN1*), cytotoxicity score (*PRF1, IFNG, FASLG, GZMA, GZMB, GZMH, GZMK, GNLY*). Importantly, we did not include in cytotoxicity score the expression of effector molecules that could be transcriptionally active in bystander virus-specific TILs, as determined in (14). The same scoring procedure was applied on T_{Ex} clonotypes to quantify the expression of gene-signatures of T cell subsets with validated specificity for tumor antigens, as reported in human (14, 21) or mouse studies (22) (Fig. S4D). Of note, in our dataset T_{PE} CD8+ TILs were identified based on elevated expression of exhaustion markers in the presence of low expression of memory-related markers (Fig 2B). Evaluation of stem-cell and memory features across exhausted clones with putative tumor reactivity further validated their classification (Fig. S4D). However, the high expression of effector cytokines (Fig. S3D) and poor TCR overlap with remaining T_{TE} populations (Fig. S4C) indicate that this cluster is also composed by CD8+ TILs with non-T_{PE} features, and therefore we classified it as “T_{PE}-like”. Clusters and TCR clonotypes were classified in meta-clusters (T_{NExM}, T_{Ex} or others) as reported in Supplementary Methods.

Multiplexed immunofluorescence

The staining procedure, including target antigens, antibody clones, dilutions, and antigen retrieval conditions is reported in Supplementary Methods. Image acquisition was performed using the Vectra Polaris multispectral imaging platform (Vectra Polaris, Akoya Biosciences). Of note, CD103 was chosen to identify TRM cells *in vivo* due to its well-defined expression in TRM populations, and the lack of an experimentally-validated antibody against ZNF683 for IF. Areas with non-tumor or residual normal tissue were excluded from the analysis.

Representative regions of interest were selected under pathologist supervision, 6 fields of view (FOV) were acquired at 20x resolution. Once the FOV were spectrally unmixed, cell identification was performed using supervised machine learning algorithms within Inform 2.4 (Akoya, Supplementary Methods). Thresholds for "positive" staining and the accuracy of phenotypic algorithms were optimized and confirmed under pathologist supervision for each case. Quantification of cell populations per mm^2 are reported in Data File S6.

Statistical analyses

The following statistical tests were used in this study to describe patient characteristics and outcomes: 1) Frequencies were used to describe the distribution of characteristics and outcome measures presented by categorical level variables, 2) Shapiro-Wilk's test was used for testing normal distribution assumption for continuous level variables. Median and range were used to describe non-normally distributed variables, 3) Chi square test or Fishers exact test and Wilcoxon rank sum test were used to explore differences in the distribution of categorical and continuous level variables respectively, between groups of interest, 4) Proportion difference and 95% CI were calculated using Jeffrey's formula and used as measures of effect size for categorical variables and median difference and 95% CI calculated using Hodges-Lehman method were used as measure of effect size for continuous level variables, 5) Kaplan-Meier product limit method of survival and Log-rank test were used to explore and compare differences in OS and PFS between groups of interest. 2-year survival rates and 95% CI were estimated and compared. All tests were two-sided. Analyses were performed using STATA v13.1 and SPSS v28.

The following statistical tests were used in this study for T cell analyses, as indicated throughout the text: 1) Spearman's correlation coefficients and associated two-sided *P* values were computed using GraphPad Prism 9 to test the null hypothesis that the correlation coefficient is zero. (2) two tailed Fisher's exact test were performed in R to calculate significance of deviation of a distribution from the null hypothesis of no differential distribution. (3) Wilcoxon rank sum test was performed in R for data with high variance to test whether mean gene-expression ranks differ among 2 groups of cells. (4) Ratio-paired parametric *t*-tests were performed using the GraphPad Prism 9 software, to obtain the two-sided *P* value of the null hypothesis that the paired values of two groups (pre-post samples) have ratio equal to 1. (5) unpaired *t* with or without *Welch's* correction tests were performed using the GraphPad Prism 9 software to obtain the two-sided *P* value of the null hypothesis that the two groups (R vs RN) have equal means. (6) Mann-Whitney tests were performed using the GraphPad Prism 9 software to compare ranks of measurements among group of patients with different pTR. No statistical methods were used to predetermine sample size. The experiments were not randomized and investigators were not blinded to allocation during experiments and outcome assessment. Patients were selected for scRNA-seq and scTCR-seq based on amount of available tumor material.

Supplementary Material

Refer to Web version on PubMed Central for supplementary material.

Acknowledgements

We thank all patients and their families for their participation in this study. We recognize the support of the Alvin J. Siteman Cancer Center at Washington University School of Medicine and Barnes-Jewish Hospital in St. Louis, Missouri and the Clinical Trials Core. The authors thanks all the members of the Wu lab for productive discussions and critical reading of the manuscript.

Funding:

R. Uppaluri is funded by the National Cancer Institute, the National Institute for Dental and Craniofacial Research (NIH/NCI/NIDCR U01DE029188 and NIH/NIDCR R01DE027736) and a V Foundation Translational Research Award. Single-cell data acquisition was supported by Robert A. and Renee E. Belfer Foundation and Expect Miracles Foundation. Clinical trial support was through a Merck Investigator Studies Program award to R. Uppaluri/D.R. Adkins. The Siteman Cancer Center is supported in part by NCI Cancer Center Support Grant #P30 CA91842.

L.P. is a Scholar of the American Society of Hematology (ASH) and a BIH Charité Digital Clinician Scientist.

References and Notes

1. Mody MD, Rocco JW, Yom SS, Haddad RI, Saba NF, Head and neck cancer. Lancet 398, 2289–2299 (2021). [PubMed: 34562395]
2. Egloff AM, Uppaluri R, Preoperative immunotherapy for head and neck cancers: state of art. Curr Opin Oncol (2022), doi:10.1097/CCO.0000000000000826.
3. Uppaluri R, Campbell KM, Egloff AM, Zolkind P, Skidmore ZL, Nussenbaum B, Paniello RC, Rich JT, Jackson R, Pipkorn P, Michel LS, Ley J, Oppelt P, Dunn GP, Barnell EK, Spies NC, Lin T, Li T, Mulder DT, Hanna Y, Cirlan I, Pugh TJ, Mudianto T, Riley R, Zhou L, Jo VY, Stachler MD, Hanna GJ, Kass J, Haddad R, Schoenfeld JD, Gjini E, Lako A, Thorstad W, Gay HA, Daly M, Rodig SJ, Hagemann IS, Kallogjeri D, Piccirillo JF, Chernock RD, Griffith M, Griffith OL, Adkins DR, Neoadjuvant and Adjuvant Pembrolizumab in Resectable Locally Advanced, Human Papillomavirus-Unrelated Head and Neck Cancer: A Multicenter, Phase II Trial. Clin Cancer Res 26, 5140–5152 (2020). [PubMed: 32665297]
4. Wise-Draper TM, Gulati S, Palackdharry S, Hinrichs BH, Worden FP, Old MO, Dunlap NE, Kaczmar JM, Patil Y, Riaz MK, Tang A, Mark J, Zender C, Gillenwater AM, Bell D, Kurtzweil N, Mathews M, Allen CL, Mierzwa ML, Casper K, Jandarov R, Medvedovic M, Lee JJ, Harun N, Takiar V, Gillison M, Phase II Clinical Trial of Neoadjuvant and Adjuvant Pembrolizumab in Resectable Local-Regionally Advanced Head and Neck Squamous Cell Carcinoma. Clin Cancer Res 28, 1345–1352 (2022). [PubMed: 35338369]
5. Luginbuhl AJ, Johnson JM, Harshyne LA, Linnenbach AJ, Shukla SK, Alnemri A, Kumar G, Cognetti DM, Curry JM, Kotlov N, Antysheva Z, Degryse S, Mannion K, Gibson MK, Netterville J, Brown B, Axelrod R, Zinner R, Tuluc M, Gargano S, Leiby BE, Shimada A, Mahoney MG, Martinez-Outschoorn U, Rodeck U, Kim YJ, South AP, Argiris A, Tadalafil Enhances Immune Signatures in Response to Neoadjuvant Nivolumab in Resectable Head and Neck Squamous Cell Carcinoma. Clin Cancer Res 28, 915–927 (2022). [PubMed: 34911681]
6. Vos JL, Elbers JBW, Krijgsman O, Traets JJH, Qiao X, van der Leun AM, Lubeck Y, Seignette IM, Smit LA, Willems SM, van den Brekel MWM, Dirven R, Baris Karakullukcu M, Karssemakers L, Klop WMC, Lohuis PJFM, Schreuder WH, Smeele LE, van der Velden L-A, Bing Tan I, Onderwater S, Jasperse B, Vogel WV, Al-Mamgani A, Keijser A, van der Noort V, Broeks A, Hooijberg E, Peeper DS, Schumacher TN, Blank CU, de Boer JP, Haanen JBAG, Zuur CL, Neoadjuvant immunotherapy with nivolumab and ipilimumab induces major pathological responses in patients with head and neck squamous cell carcinoma. Nat Commun 12, 7348 (2021). [PubMed: 34937871]
7. Schoenfeld JD, Hanna GJ, Jo VY, Rawal B, Chen Y-H, Catalano PS, Lako A, Ciantra Z, Weirather JL, Criscitiello S, Luoma A, Chau N, Lorch J, Kass JI, Annino D, Goguen L, Desai A, Ross B, Shah HJ, Jacene HA, Margalit DN, Tishler RB, Wucherpfennig KW, Rodig SJ, Uppaluri R, Haddad RI, Neoadjuvant Nivolumab or Nivolumab Plus Ipilimumab in Untreated Oral Cavity Squamous Cell

Carcinoma: A Phase 2 Open-Label Randomized Clinical Trial. JAMA Oncol 6, 1563–1570 (2020). [PubMed: 32852531]

8. Hanna GJ, O'Neill A, Shin K-Y, Wong K, Jo VY, Quinn CT, Cutler JM, Flynn M, Lizotte PH, Annino DJ, Goguen LA, Kass JI, Rettig EM, Sethi RKV, Lorch JH, Schoenfeld JD, Margalit DN, Tishler RB, Everett PC, Desai AM, Cavanaugh ME, Paweletz CP, Egloff AM, Uppaluri R, Haddad RI, Neoadjuvant and Adjuvant Nivolumab and Lirilumab in Patients with Recurrent, Resectable Squamous Cell Carcinoma of the Head and Neck. Clin Cancer Res 28, 468–478 (2022). [PubMed: 34667025]
9. Huang AC, Postow MA, Orlowski RJ, Mick R, Bengsch B, Manne S, Xu W, Harmon S, Giles JR, Wenz B, Adamow M, Kuk D, Panageas KS, Carrera C, Wong P, Quagliarello F, Wubbenhorst B, D'Andrea K, Pauken KE, Herati RS, Staupe RP, Schenkel JM, McGettigan S, Kothari S, George SM, Vonderheide RH, Amaravadi RK, Karakousis GC, Schuchter LM, Xu X, Nathanson KL, Wolchok JD, Gangadhar TC, Wherry EJ, T-cell invigoration to tumour burden ratio associated with anti-PD-1 response. Nature 545, 60–65 (2017). [PubMed: 28397821]
10. Liu B, Hu X, Feng K, Gao R, Xue Z, Zhang S, Zhang Y, Corse E, Hu Y, Han W, Zhang Z, Temporal single-cell tracing reveals clonal revival and expansion of precursor exhausted T cells during anti-PD-1 therapy in lung cancer. Nat Cancer 3, 108–121 (2022). [PubMed: 35121991]
11. Yost KE, Satpathy AT, Wells DK, Qi Y, Wang C, Kageyama R, McNamara KL, Granja JM, Sarin KY, Brown RA, Gupta RK, Curtis C, Bucktrout SL, Davis MM, Chang ALS, Chang HY, Clonal replacement of tumor-specific T cells following PD-1 blockade. Nat Med 25, 1251–1259 (2019). [PubMed: 31359002]
12. Luoma AM, Suo S, Wang Y, Gunasti L, Porter CBM, Nabilsi N, Tadros J, Ferretti AP, Liao S, Gurer C, Chen Y-H, Criscitiello S, Ricker CA, Dionne D, Rozenblatt-Rosen O, Uppaluri R, Haddad RI, Ashenberg O, Regev A, Van Allen EM, MacBeath G, Schoenfeld JD, Wucherpfennig KW, Tissue-resident memory and circulating T cells are early responders to pre-surgical cancer immunotherapy. Cell 185, 2918–2935.e29 (2022). [PubMed: 35803260]
13. Oh DY, Kwek SS, Raju SS, Li T, McCarthy E, Chow E, Aran D, Ilano A, Pai C-CS, Rancan C, Allaire K, Burra A, Sun Y, Spitzer MH, Mangul S, Porten S, Meng MV, Friedlander TW, Ye CJ, Fong L, Intratumoral CD4+ T Cells Mediate Anti-tumor Cytotoxicity in Human Bladder Cancer. Cell 181, 1612–1625.e13 (2020). [PubMed: 32497499]
14. Oliveira G, Stromhaug K, Klaeger S, Kula T, Frederick DT, Le PM, Forman J, Huang T, Li S, Zhang W, Xu Q, Cieri N, Clauser KR, Shukla SA, Neuberg D, Justesen S, MacBeath G, Carr SA, Fritsch EF, Hacohen N, Sade-Feldman M, Livak KJ, Boland GM, Ott PA, Keskin DB, Wu CJ, Phenotype, specificity and avidity of antitumour CD8+ T cells in melanoma. Nature 596, 119–125 (2021). [PubMed: 34290406]
15. Mackay LK, Minnich M, Kragten NAM, Liao Y, Nota B, Seillet C, Zaid A, Man K, Preston S, Freestone D, Braun A, Wynne-Jones E, Behr FM, Stark R, Pellicci DG, Godfrey DI, Belz GT, Pellegrini M, Gebhardt T, Busslinger M, Shi W, Carbone FR, van Lier RAW, Kallies A, van Gisbergen KPJM, Hobit and Blimp1 instruct a universal transcriptional program of tissue residency in lymphocytes. Science 352, 459–463 (2016). [PubMed: 27102484]
16. Parga-Vidal L, Behr FM, Kragten NAM, Nota B, Wesselink TH, Kavazović I, Covill LE, Schuller MBP, Bryceson YT, Wensveen FM, van Lier RAW, van Dam TJP, Stark R, van Gisbergen KPJM, Hobit identifies tissue-resident memory T cell precursors that are regulated by Eomes. Sci Immunol 6, eabg3533 (2021). [PubMed: 34417257]
17. van der Leun AM, Thommen DS, Schumacher TN, CD8+ T cell states in human cancer: insights from single-cell analysis. Nat Rev Cancer 20, 218–232 (2020). [PubMed: 32024970]
18. Wolfl M, Kuball J, Ho WY, Nguyen H, Manley TJ, Bleakley M, Greenberg PD, Activation-induced expression of CD137 permits detection, isolation, and expansion of the full repertoire of CD8+ T cells responding to antigen without requiring knowledge of epitope specificities. Blood 110, 201–210 (2007). [PubMed: 17371945]
19. Simoni Y, Becht E, Fehlings M, Loh CY, Koo S-L, Teng KWW, Yeong JPS, Nahar R, Zhang T, Kared H, Duan K, Ang N, Poidinger M, Lee YY, Larbi A, Khng AJ, Tan E, Fu C, Mathew R, Teo M, Lim WT, Toh CK, Ong B-H, Koh T, Hillmer AM, Takano A, Lim TKH, Tan EH, Zhai W, Tan DSW, Tan IB, Newell EW, Bystander CD8+ T cells are abundant and phenotypically distinct in human tumour infiltrates. Nature 557, 575–579 (2018). [PubMed: 29769722]

20. Caushi JX, Zhang J, Ji Z, Vaghasia A, Zhang B, Hsiue EH-C, Mog BJ, Hou W, Justesen S, Blosser R, Tam A, Anagnostou V, Cottrell TR, Guo H, Chan HY, Singh D, Thapa S, Dykema AG, Burman P, Choudhury B, Aparicio L, Cheung LS, Lanis M, Belcaid Z, El Asmar M, Illei PB, Wang R, Meyers J, Schuebel K, Gupta A, Skaist A, Wheelan S, Naidoo J, Marrone KA, Brock M, Ha J, Bush EL, Park BJ, Bott M, Jones DR, Reuss JE, Velculescu VE, Chaft JE, Kinzler KW, Zhou S, Vogelstein B, Taube JM, Hellmann MD, Brahmer JR, Merghoub T, Forde PM, Yegnasubramanian S, Ji H, Pardoll DM, Smith KN, Transcriptional programs of neoantigen-specific TIL in anti-PD-1-treated lung cancers. Nature 596, 126–132 (2021). [PubMed: 34290408]

21. Eberhardt CS, Kissick HT, Patel MR, Cardenas MA, Prokhnevska N, Obeng RC, Nasti TH, Griffith CC, Im SJ, Wang X, Shin DM, Carrington M, Chen ZG, Sidney J, Sette A, Saba NF, Wieland A, Ahmed R, Functional HPV-specific PD-1+ stem-like CD8 T cells in head and neck cancer. Nature 597, 279–284 (2021). [PubMed: 34471285]

22. Miller BC, Sen DR, Al Abosy R, Bi K, Virkud YV, LaFleur MW, Yates KB, Lako A, Felt K, Naik GS, Manos M, Gjini E, Kuchroo JR, Ishizuka JJ, Collier JL, Griffin GK, Maleri S, Comstock DE, Weiss SA, Brown FD, Panda A, Zimmer MD, Manguso RT, Hodi FS, Rodig SJ, Sharpe AH, Haining WN, Subsets of exhausted CD8+ T cells differentially mediate tumor control and respond to checkpoint blockade. Nat Immunol 20, 326–336 (2019). [PubMed: 30778252]

23. Lowery FJ, Krishna S, Yossef R, Parikh NB, Chatani PD, Zacharakis N, Parkhurst MR, Levin N, Sindiri S, Sachs A, Hitscherich KJ, Yu Z, Vale NR, Lu Y-C, Zheng Z, Jia L, Gartner JJ, Hill VK, Copeland AR, Nah SK, Masi RV, Gasmi B, Kivitz S, Paria BC, Florentin M, Kim SP, Hanada K-I, Li YF, Ngo LT, Ray S, Shindorf ML, Levi ST, Shepherd R, Toy C, Parikh AY, Prickett TD, Kelly MC, Beyer R, Goff SL, Yang JC, Robbins PF, Rosenberg SA, Molecular signatures of antitumor neoantigen-reactive T cells from metastatic human cancers. Science , eabl5447 (2022).

24. Oliveira et al. , Landscape of helper and regulatory antitumor CD4+ T cells in melanoma. In press, Nature.

25. Guo X, Zhang Y, Zheng L, Zheng C, Song J, Zhang Q, Kang B, Liu Z, Jin L, Xing R, Gao R, Zhang L, Dong M, Hu X, Ren X, Kirchhoff D, Roider HG, Yan T, Zhang Z, Global characterization of T cells in non-small-cell lung cancer by single-cell sequencing. Nat Med 24, 978–985 (2018). [PubMed: 29942094]

26. Pauken KE, Sammons MA, Odorizzi PM, Manne S, Godec J, Khan O, Drake AM, Chen Z, Sen DR, Kurachi M, Barnitz RA, Bartman C, Bengsch B, Huang AC, Schenkel JM, Vahedi G, Haining WN, Berger SL, Wherry EJ, Epigenetic stability of exhausted T cells limits durability of reinvigoration by PD-1 blockade. Science 354, 1160–1165 (2016). [PubMed: 27789795]

27. Subramanian A, Tamayo P, Mootha VK, Mukherjee S, Ebert BL, Gillette MA, Paulovich A, Pomeroy SL, Golub TR, Lander ES, Mesirov JP, Gene set enrichment analysis: a knowledge-based approach for interpreting genome-wide expression profiles. Proc Natl Acad Sci U S A 102, 15545–15550 (2005). [PubMed: 16199517]

28. Mackay LK, Rahimpour A, Ma JZ, Collins N, Stock AT, Hafon M-L, Vega-Ramos J, Lauzurica P, Mueller SN, Stefanovic T, Tscharke DC, Heath WR, Inouye M, Carbone FR, Gebhardt T, The developmental pathway for CD103(+)CD8+ tissue-resident memory T cells of skin. Nat Immunol 14, 1294–1301 (2013). [PubMed: 24162776]

29. Duhen T, Duhen R, Montler R, Moses J, Moudgil T, de Miranda NF, Goodall CP, Blair TC, Fox BA, McDermott JE, Chang S-C, Grunkemeier G, Leidner R, Bell RB, Weinberg AD, Co-expression of CD39 and CD103 identifies tumor-reactive CD8 T cells in human solid tumors. Nat Commun 9, 2724 (2018). [PubMed: 30006565]

30. Liu S, Knochelmann HM, Lomeli SH, Hong A, Richardson M, Yang Z, Lim RJ, Wang Y, Dumitras C, Krysan K, Timmers C, Romeo MJ, Krieg C, O'Quinn EC, Horton JD, Dubinett SM, Paulos CM, Neskey DM, Lo RS, Response and recurrence correlates in individuals treated with neoadjuvant anti-PD-1 therapy for resectable oral cavity squamous cell carcinoma. Cell Rep Med 2, 100411 (2021). [PubMed: 34755131]

31. Sade-Feldman M, Yizhak K, Bjorgaard SL, Ray JP, de Boer CG, Jenkins RW, Lieb DJ, Chen JH, Frederick DT, Barzily-Rokni M, Freeman SS, Reuben A, Hoover PJ, Villani A-C, Ivanova E, Portell A, Lizotte PH, Aref AR, Eliane J-P, Hammond MR, Vitzthum H, Blackmon SM, Li B, Gopalakrishnan V, Reddy SM, Cooper ZA, Paweletz CP, Barbie DA, Stemmer-Rachamimov A, Flaherty KT, Wargo JA, Boland GM, Sullivan RJ, Getz G, Hacohen N, Defining T Cell States

Associated with Response to Checkpoint Immunotherapy in Melanoma. Cell 176, 404 (2019). [PubMed: 30633907]

32. Anadon CM, Yu X, Hänggi K, Biswas S, Chaurio RA, Martin A, Payne KK, Mandal G, Innamarato P, Harro CM, Mine JA, Sprenger KB, Cortina C, Powers JJ, Costich TL, Perez BA, Gatenbee CD, Prabhakaran S, Marchion D, Heemskerk MHM, Curiel TJ, Anderson AR, Wenham RM, Rodriguez PC, Conejo-Garcia JR, Ovarian cancer immunogenicity is governed by a narrow subset of progenitor tissue-resident memory T cells. Cancer Cell 40, 545–557.e13 (2022). [PubMed: 35427494]
33. Kersten K, Hu KH, Combes AJ, Samad B, Harwin T, Ray A, Rao AA, Cai E, Marchuk K, Artichoker J, Courau T, Shi Q, Belk J, Satpathy AT, Krummel MF, Spatiotemporal co-dependency between macrophages and exhausted CD8+ T cells in cancer. Cancer Cell 40, 624–638.e9 (2022). [PubMed: 35623342]
34. Gabrilovich DI, Nagaraj S, Myeloid-derived suppressor cells as regulators of the immune system. Nat Rev Immunol 9, 162–174 (2009). [PubMed: 19197294]
35. Schumacher TN, Thommen DS, Tertiary lymphoid structures in cancer. Science 375, eabf9419 (2022). [PubMed: 34990248]
36. Tosi A, Parisatto B, Menegaldo A, Spinato G, Guido M, Del Mistro A, Bussani R, Zanconati F, Tofanelli M, Tirelli G, Boscolo-Rizzo P, Rosato A, The immune microenvironment of HPV-positive and HPV-negative oropharyngeal squamous cell carcinoma: a multiparametric quantitative and spatial analysis unveils a rationale to target treatment-naïve tumors with immune checkpoint inhibitors. J Exp Clin Cancer Res 41, 279 (2022). [PubMed: 36123711]
37. Milner JJ, Goldrath AW, Transcriptional programming of tissue-resident memory CD8+ T cells. Curr Opin Immunol 51, 162–169 (2018). [PubMed: 29621697]
38. Okła K, Farber DL, Zou W, Tissue-resident memory T cells in tumor immunity and immunotherapy. J Exp Med 218, e20201605 (2021). [PubMed: 33755718]
39. Szabo PA, Miron M, Farber DL, Location, location, location: Tissue resident memory T cells in mice and humans. Sci Immunol 4, eaas9673 (2019). [PubMed: 30952804]
40. Banchereau R, Chitre AS, Scherl A, Wu TD, Patil NS, de Almeida P, Kadel Iii EE, Madireddi S, Au-Yeung A, Takahashi C, Chen Y-J, Modrusan Z, McBride J, Nersesian R, El-Gabry EA, Robida MD, Hung JC, Kowanetz M, Zou W, McCleland M, Caplazi P, Eshgi ST, Koeppen H, Hegde PS, Mellman I, Mathews WR, Powles T, Mariathasan S, Grogan J, O'Gorman WE, Intratumoral CD103+ CD8+ T cells predict response to PD-L1 blockade. J Immunother Cancer 9, e002231 (2021). [PubMed: 33827905]
41. Savas P, Virassamy B, Ye C, Salim A, Mintoff CP, Caramia F, Salgado R, Byrne DJ, Teo ZL, Dushyanthen S, Byrne A, Wein L, Luen SJ, Poliness C, Nightingale SS, Skandarajah AS, Gyorki DE, Thornton CM, Beavis PA, Fox SB, Kathleen Cuningham Foundation Consortium for Research into Familial Breast Cancer (kConFab), Darcy PK, Speed TP, Mackay LK, Neeson PJ, Loi S, Single-cell profiling of breast cancer T cells reveals a tissue-resident memory subset associated with improved prognosis. Nat Med 24, 986–993 (2018). [PubMed: 29942092]
42. Clarke J, Panwar B, Madrigal A, Singh D, Gujar R, Wood O, Chee SJ, Eschweiler S, King EV, Awad AS, Hanley CJ, McCann KJ, Bhattacharyya S, Woo E, Alzetani A, Seumois G, Thomas GJ, Ganesan A-P, Friedmann PS, Sanchez-Elsner T, Ay F, Ottensmeier CH, Vijayanand P, Single-cell transcriptomic analysis of tissue-resident memory T cells in human lung cancer. J Exp Med 216, 2128–2149 (2019). [PubMed: 31227543]
43. Egelston CA, Avalos C, Tu TY, Rosario A, Wang R, Solomon S, Srinivasan G, Nelson MS, Huang Y, Lim MH, Simons DL, He T-F, Yim JH, Kruper L, Mortimer J, Yost S, Guo W, Ruel C, Frankel PH, Yuan Y, Lee PP, Resident memory CD8+ T cells within cancer islands mediate survival in breast cancer patients. JCI Insight 4, 130000 (2019). [PubMed: 31465302]
44. Dindo D, Demartines N, Clavien P-A, Classification of surgical complications: a new proposal with evaluation in a cohort of 6336 patients and results of a survey. Ann Surg 240, 205–213 (2004). [PubMed: 15273542]
45. Stuart T, Butler A, Hoffman P, Hafemeister C, Papalexi E, Mauck WM, Hao Y, Stoeckius M, Smibert P, Satija R, Comprehensive Integration of Single-Cell Data. Cell 177, 1888–1902.e21 (2019). [PubMed: 31178118]

46. Korsunsky I, Millard N, Fan J, Slowikowski K, Zhang F, Wei K, Baglaenko Y, Brenner M, Loh P-R, Raychaudhuri S, Fast, sensitive and accurate integration of single-cell data with Harmony. Nat Methods 16, 1289–1296 (2019). [PubMed: 31740819]

47. Wu TD, Madireddi S, de Almeida PE, Banchereau R, Chen Y-JJ, Chitre AS, Chiang EY, Iftikhar H, O'Gorman WE, Au-Yeung A, Takahashi C, Goldstein LD, Poon C, Keerthivasan S, de Almeida Nagata DE, Du X, Lee H-M, Banta KL, Mariathasan S, Das Thakur M, Huseni MA, Ballinger M, Estay I, Caplazi P, Modrusan Z, Delamarre L, Mellman I, Bourgon R, Grogan JL, Peripheral T cell expansion predicts tumour infiltration and clinical response. Nature 579, 274–278 (2020). [PubMed: 32103181]

48. Nguyen H, Tran D, Galazka JM, Costes SV, Beheshti A, Petereit J, Draghici S, Nguyen T, CPA: a web-based platform for consensus pathway analysis and interactive visualization. Nucleic Acids Res 49, W114–W124 (2021). [PubMed: 34037798]

49. Patro R, Duggal G, Love MI, Irizarry RA, Kingsford C, Salmon provides fast and bias-aware quantification of transcript expression. Nat Methods 14, 417–419 (2017). [PubMed: 28263959]

50. Soneson C, Love MI, Robinson MD, Differential analyses for RNA-seq: transcript-level estimates improve gene-level inferences. F1000Res 4, 1521 (2015). [PubMed: 26925227]

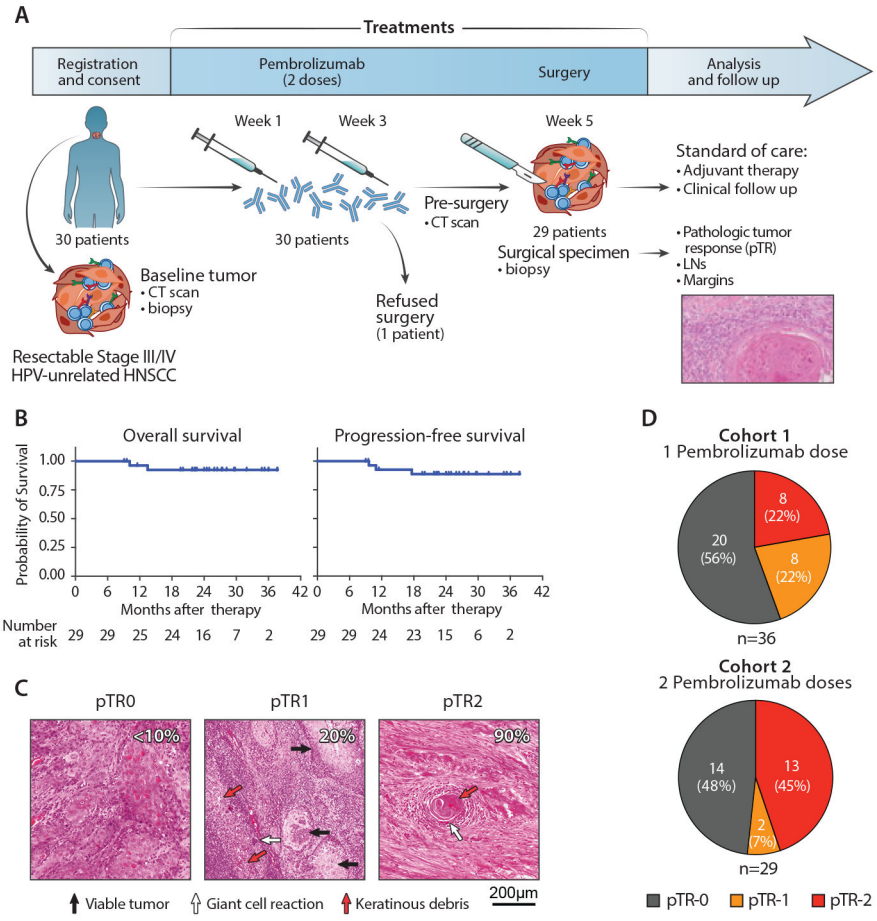

Fig. 1. Outcome of neoadjuvant PD-1 blockade in patients with HNSCC.

(**A**) Scheme of treatment and outcome analysis. After enrollment and screening, patients with HNSCC received 2 doses of anti-PD-1 before surgery. Resected tumors specimens were assessed for the rate of response as part of pathologic staging. (**B**) Kaplan-Meier curves estimating the overall survival (left) and progression-free survival (left) of 29 patients with HNSCC who received 2 doses of neoadjuvant PD-1 blockade and surgery. Time from surgical resection is presented as months elapsed. The number of evaluated at-risk patients is reported below each graph. (**C**) Hematoxylin-eosin staining of tumor biopsies collected at surgery from 3 representative patients with different levels of pTR (quantification indicated by white numbers). Arrows - representative areas with viable tumor cells (black), giant cell/histiocytic reaction (white) or necrotic cells/keratinous debris (red). (**D**) Rates of pTR in patients treated with 2 neoadjuvant doses of anti-PD-1 antibodies (this study, right, n=29) compared with patients who received a single dose, as previously reported (3) (left).

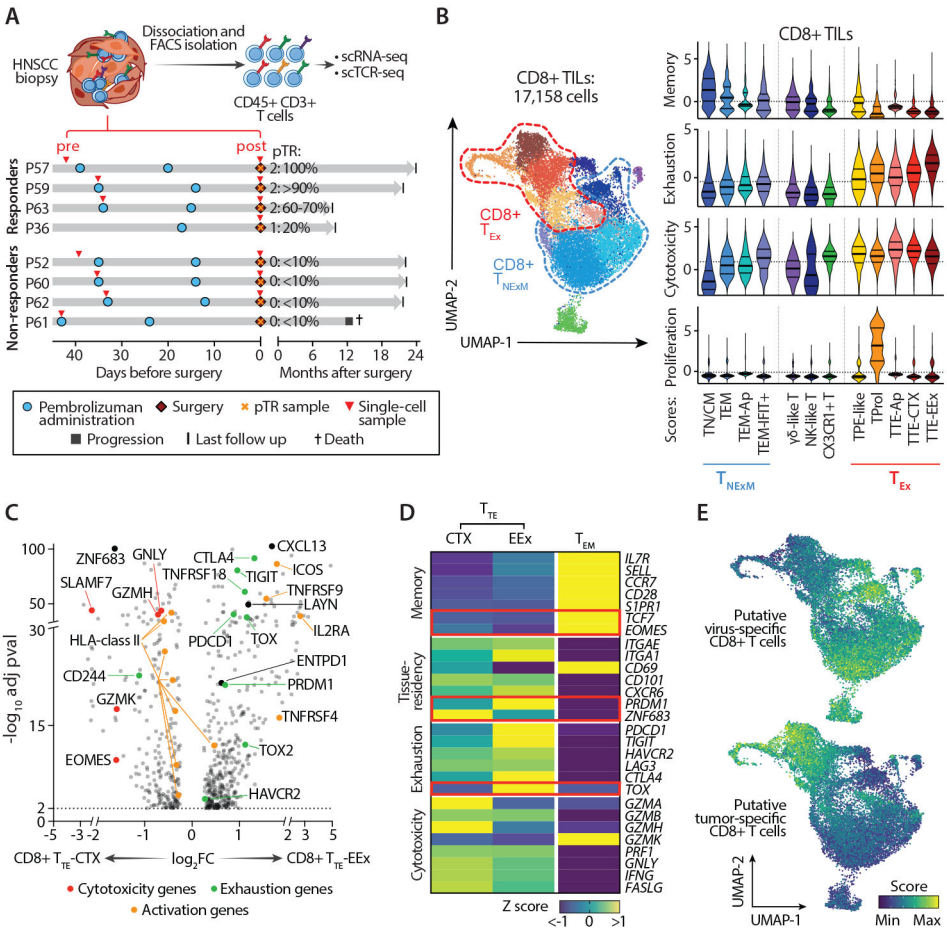

Fig. 2. Characterization of CD8+ TILs in HNSCC.

(**A**) Scheme of collection and processing of TILs for single-cell analysis. Clinical courses of 4 Rs and 4 NRs are represented. Red arrows - time of collection of the tumor biopsies profiled at baseline (pre) or at surgery after PD-1 blockade (post). pTR assessed at tumor resection is reported. (**B**) Classification of CD8+ HNSCC-TILs. UMAP of the transcriptionally-defined clusters from the scRNA-seq data (left), as denoted by colors. Right plots - The inferred cell states (x axis), colored to match the UMAP clusters. Cells from each cell state are scored for expression of memory, exhaustion, cytotoxicity and proliferation genes (see Materials and Methods), with medians and quartiles indicated (thick and thin horizontal lines, respectively). Horizontal dashed lines - average scores within the entire dataset of CD8+ TILs. (**C**) Differentially expressed genes for all cells in CD8+ T_{TE} with cytotoxic characteristics (T_{TE}-CTX) (left) and CD8+ T_{TE} with extreme exhaustion programming (T_{TE}-EEx) (right) clusters. Dots denote genes with adj-pval<0.01 (two-sided Wilcoxon Rank Sum test). Representative genes are labeled, with colors corresponding to gene-functions (legend). (**D**) Heatmap reporting variation (expressed as Z-score) in average gene-expression measured in exhausted T_{TE}-CTX, T_{TE}-EEx or control T_{EM} CD8+ TILs. Qualitative differences are reported for representative T cell-related genes, divided based on their known function (left). Key transcriptional factors are highlighted in red. (**E**) UMAPs of CD8+ TILs colored based on enrichment of published gene-signatures

associated with CD8+TILs with validated antiviral (top) or antitumor (bottom) reactivity (14). Abbreviations: TN/CM: naïve/central memory TILs; TEM: effector memory TILs; TPE-like: enriched in progenitor exhausted TILs; TProl: proliferative TILs; TTE: terminally exhausted TILs; CTX: cytotoxic; EEx: extremely exhausted; Ap: apoptotic; T_{NExM}: non-exhausted memory TILs; T_{Ex}: Exhausted TILs.

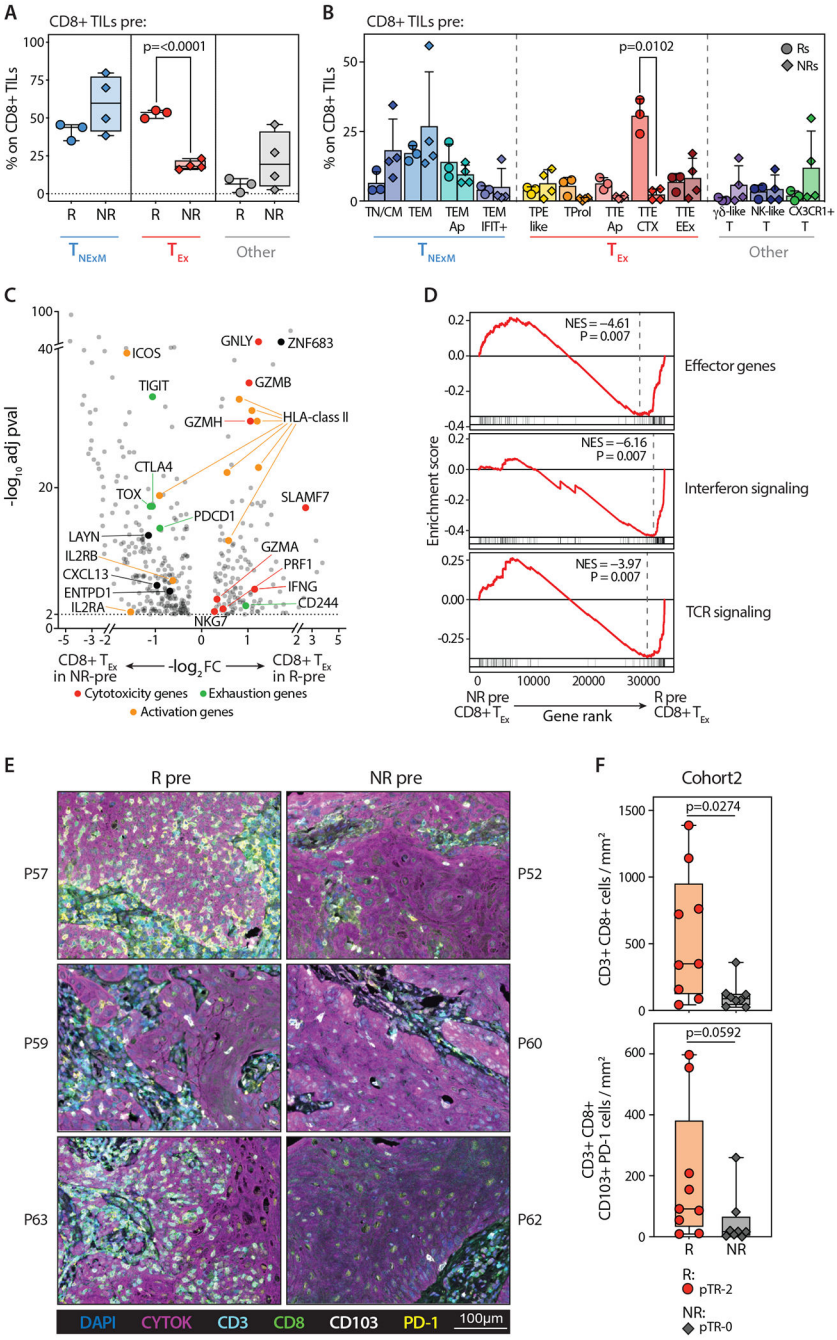

Fig. 3. CD8+ TILs before PD-1 blockade in responder and non-responder patients

(**A**) Frequencies of principal phenotypes among CD8+ TILs collected from Responders (R, circles, n=3) or Non-Responders (NR, diamonds, n=4) at pre-treatment timepoints (Pre). Box plots - median percentage of TILs with phenotypes corresponding to CD8+ non-exhausted memory cell states (T_{NExM}, blue), exhausted states (T_{Ex}, red), or unclassified clusters (Other, grey; see Fig. 2B). Whiskers: min-max values; horizontal bars: medians. Boxes: 25^{th}-75^{th} percentiles. P values: significant comparisons (two-tailed *Welch's t*-test). (**B**) Proportions of CD8+ TILs from pretreatment biopsies (pre) collected from Rs (circles,

n=3) and NRs (diamonds, n=4, Data File S4). Colors identify cell states, as inferred from cluster classification (Fig. 2B, Fig. S3) and are grouped based on association in primary clusters (x axis). P values of significant comparisons are shown, as calculated with two-tailed *Welch's t test*. (**C**) Differentially expressed genes among CD8+ T_{Ex}-TILs detected in baseline biopsies in Responders (R, right, n=3) and Non-Responders (NR, left, n=3). Dots denote genes with adj-pval<0.01 (two-sided Wilcoxon Rank Sum test). Representative genes are labeled, with colors corresponding to gene-functions (legend). Genes enriched in baseline CD8+ T_{Ex}-TILs in patients with good or poor response after PD-1 blockade were selected from this comparison ($log_2FC>1$) and included in signatures (Data File S5). (**D**) GSEA enrichment of the CD8+ T_{Ex}-TILs in pre-treatment biopsies from Rs (right, n=3) and NRs (left, n=3) for signatures of highly reactive T cells (10, 26, 27). P values were determined by one-tailed permutation test by GSEA. NES, normalized enrichment score. (**E**) Multiplexed Immunofluorescence of tumor biopsies collected prior to treatment from 3 Rs (left) and 3NRs (right) patients previously analyzed by scRNA-seq. The representative images demonstrate the pre-existing high levels of tissue resident memory-like (CD103+) and exhausted (PD1) TILs (CD3+ CD8+) in Rs within the tumor bed, marked by expression of cytokeratin (Cytok). Lower magnifications in Fig. S6B. (**F**) Quantification of CD3+ CD8+ TILs (top) or exhausted tissue-resident (PD-1+ CD103+) CD8+ TILs (bottom) infiltrating pre-treatment biopsies collected from 17 HNSCC before two doses of neoadjuvant pembrolizumab. Infiltrates were determined by enumerating the mean number of TILs cells in 6 representative 20× fields (see Material and Methods). Dots represent individual values in Responders (pTR-2, circles) and Non-Responders (pTR-0, diamonds), as reported in Data File S6. Number of analyzed patients and degree of pTR are reported in a legend (right). P values: significant comparisons calculated with two-tailed *Mann-Whitney* test.

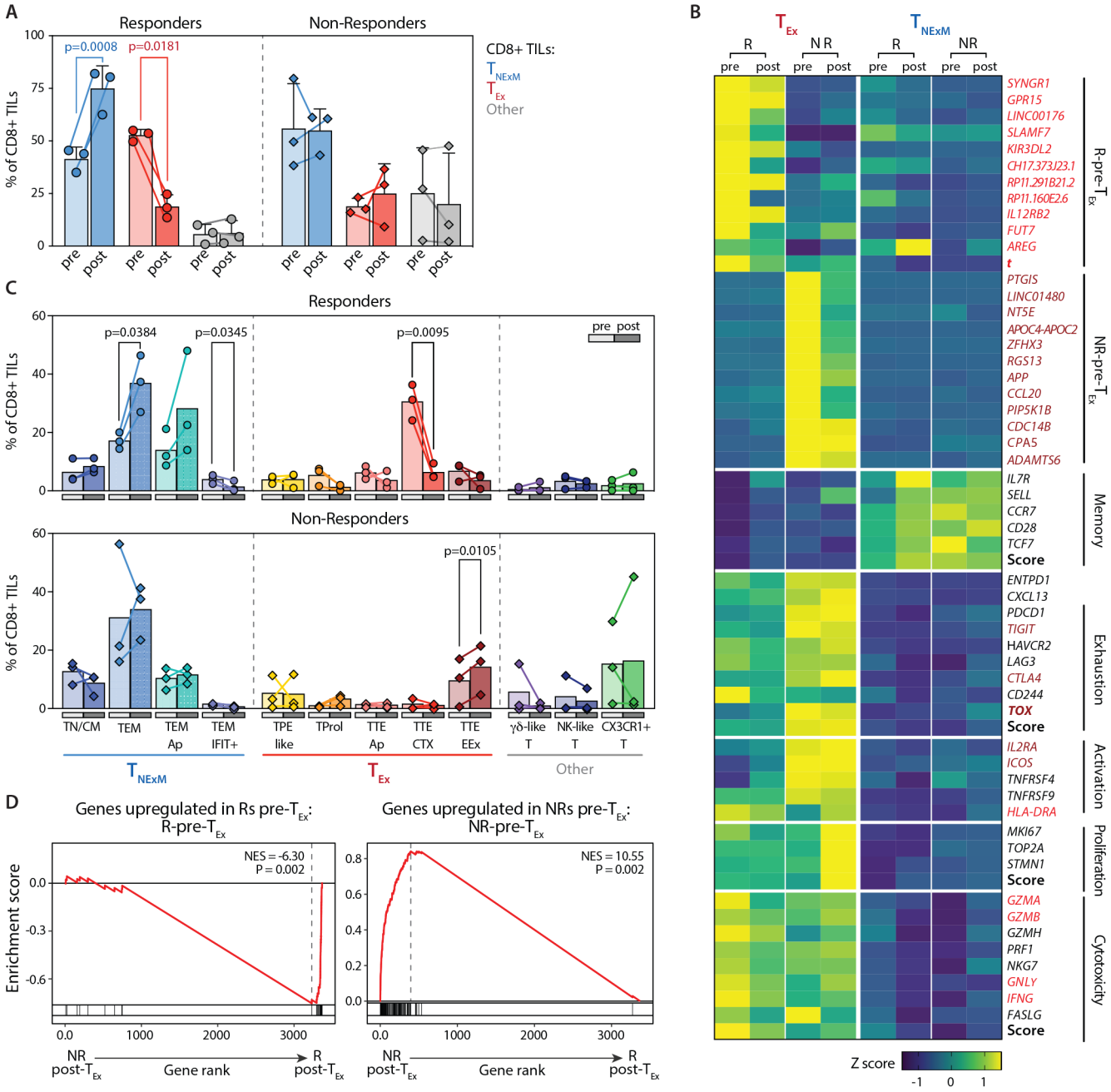

Fig. 4. Dynamics of CD8+ TIL subsets before and after PD-1 blockade in responder and non-responder patients

(**A**) Frequencies of dominant phenotypes among CD8+ TILs in HNSCC lesions collected before (pre, light colors) or after (post, dark colors) neoadjuvant PD-1 blockade (Data File S4). Dots represent individual values in Rs (n=3, circles) and NRs (n=3, diamonds), Lines connect pre-post matched evaluations for each patient. Bars - means with SD and report percentage of TILs with different primary phenotypes (T_{NExM}, blue; T_{Ex}, red; Other, grey; see Fig. 2B). P values: significant comparisons calculated with two-tailed ratio-paired *t*-test. (**B**) Heatmap reporting variation (expressed as Z-score) in average gene-expression

measured in exhausted T_{Ex} (left) or memory T_{NExM} (right) CD8+ TILs in pre- or post-treatment tumors collected from Rs and NRs. Qualitative differences are reported for top deregulated in CD8+ T_{Ex}-TILs (as established in Fig. 3C) or for representative T-cell related genes, divided based on their known function (left). Scores summarizing expression of genes in each category are depicted (bold, see Material and Methods). Genes included in signatures determined in Fig. 3C (see Data File S5) and enriched in R-Pre-T_{Ex}-TILs or NR-Pre-T_{Ex}-TILs are labeled in red and brown respectively. Key transcriptional factors are highlighted in bold. (**C**) Comparison of frequencies of CD8+ TIL-subsets analyzed before (pre: light colors) or after (post: full colors) treatment (Data File S4). Bars shows mean values, as measured in Responder (circles, top, n=3) and Non-Responders (diamonds, bottom, n=3) with available matched tumor biopsies. Colors identify cell states, which are grouped based of association in primary clusters (x axis, see Fig. 2B)). Significant P values calculated using two-sided paired *t*-test are shown. (**D**) GSEA enrichment for signatures predictive of response, enriched in R-Pre-T_{Ex}-TILs (top) or NR-Pre-T_{Ex}-TILs (bottom), as previously assessed (see panel Fig. 3C, Data File S5). Normalized enriched score (NES) is inferred comparing CD8+ T_{Ex}-TILs in post-treatment biopsies from Responders (right, n=3) or Non-Responders (left, n=3). Results show that signatures determined before therapies are still enriched in corresponding responder or non-responder patients after immunotherapy. P values were determined by one-tailed permutation test by GSEA.

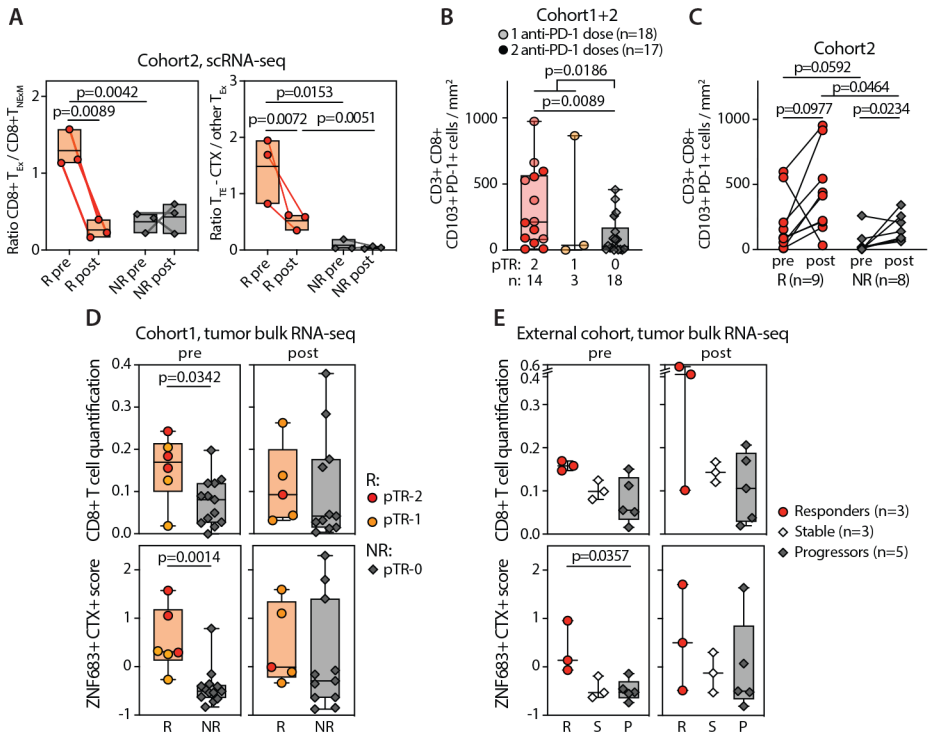

Fig. 5. Quality and quantity of TILs in pre-treatment HNSCC associate with pathologic tumor response after neoadjuvant PD-1 blockade

(**A**) Summary of quantitative and qualitative differences in putative tumor-reactive CD8+ T_{Ex}-TILs detected before or after neoadjuvant PD-1 blockade, as established in patients with available paired scRNA-seq (see Fig. 2A). Box plots - ratios (Data File S4) calculated using the frequencies of putative-tumor reactive CD8+ T_{Ex} and memory CD8+ T_{NExM} (left) or expressing the relative proportion of cytotoxic terminal exhausted CD8+ TILs (T_{TE}-CTX) over other CD8+ T_{Ex} subsets (right). Dots - individual values in Rs (n=3, circles) and NRs (n=3, diamonds), with lines connecting pre-post matched evaluations for each patient. P values: significant comparisons calculated with two-tailed unpaired *t*-test (R vs NR) or with two-tailed paired ratio *t*-test (pre vs post). (**B**) Enumeration of tissue-resident (CD103+ PD-1+) CD3+ CD8+ T cells infiltrating HNSCC specimens collected at pre-treatment timepoint from 35 patients, classified based on the extent of pathological tumor response (pTR) assessed after one (lighter shaded) or two (darker shaded) doses of neoadjuvant anti-PD-1 (cohort 1 and 2, Data File S6). Significance was calculated between Rs and NRs (pTR-1/2 vs pTR-0) or between pTR2 and pTR-0 with two-tailed *Mann-Whitney* test. (**C**) The same analysis was performed for 17 patients with available tumor specimens collected before or after two doses of pembrolizumab (cohort 2, Data File S6). Quantification of TILs was performed through immunofluorescent staining, analyzed as reported in Materials and Methods **section**. P values: significant comparisons calculated with two-tailed *Mann-Whitney* test (for group comparisons) or with two-tailed paired *t*-test (for pre vs post). (**D**) Analysis of gene-expression profile of HNSCC biopsies collected before or after neoadjuvant PD-1 blockade in patients treated with a single dose of pembrolizumab (cohort 1), as previously reported (3). Tumor bulk RNA-seq was analyzed as described in Materials and Methods section, to quantify CD8+ T cells (top) or to evaluate the level of expression

of *ZNF683* and cytotoxicity (CTX) genes before (pre, left) or after (post, right) neoadjuvant immunotherapy (Data File S7). The same analysis is performed on RNA-seq data available from 11 HNSCC biopsies collected before or after 3 doses of nivolumab (**E**), as reported in (30). P values: significant comparisons calculated with two-tailed *Mann-Whitney* test. In all the panels, dots represent values from individual patients, with colors depicting the level of pTR (panels A-D) or radiographic reduction of tumor (panel E, as established in (30)) measured after neoadjuvant immunotherapy. For column plots: boxes: 25^{th}-75^{th} percentiles; whiskers: min-max values; horizontal lines: media values.

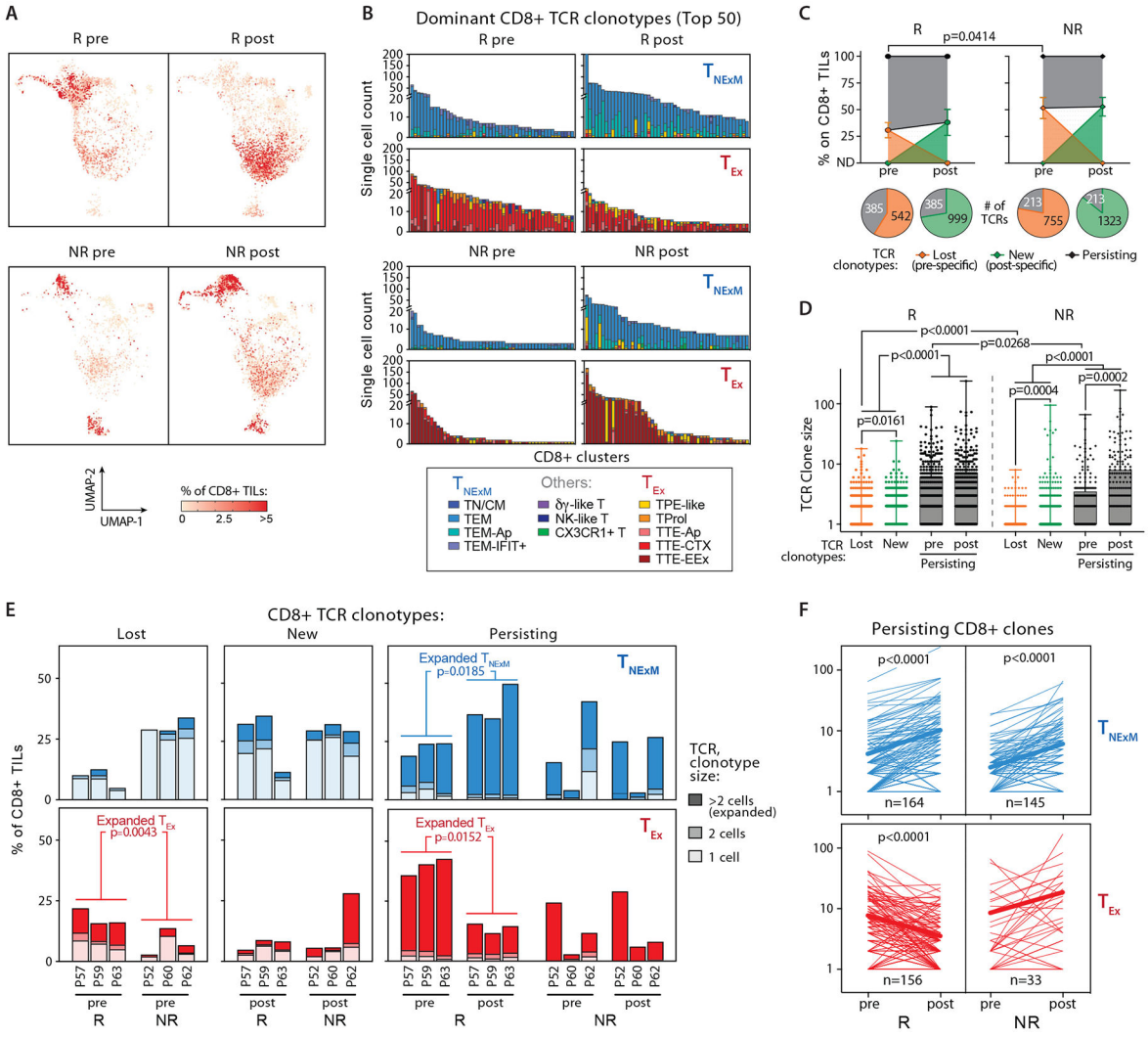

Fig. 6. Clonal dynamics of CD8+ TCR-clonotypes before and after PD1-1 blockade

(**A**) UMAP of CD8+ TILs based on intra-patient TCR clone frequency (defined through scTCR-seq) to represent clonally expanded CD8+ T cells. TCR clonotypes in 3 Rs (top) and 3 NRs (bottom) with matched biopsies collected before (pre) and (post) anti-PD1 therapy are shown. (**B**) Cluster distribution of the top 50 CD8+ TCR clonotypes classified as T_{NExM} or T_{Ex}, sequenced in pre-post therapy tumor biopsies from 3 Rs (top) and 3 NRs (bottom). Colors denote cell states inferred from scRNA-seq (see Fig. 2B), as delineated within the legend (bottom). (**C**) Overall frequencies of CD8+ TCR clonotypes, classified as Lost (orange), New (green) or Persisting (black) based on detection in pre and/or post therapy biopsies. Dots depict mean values with standard deviations, as assessed in 3 Rs (left) and 3 NRs (right) before (pre) or after (post) anti-PD-1 immunotherapy. P value reports significant differences, as established using two-tailed *t*-test. For each timepoint, bottom pies report the total number of TCR clonotypes for each category (Data File S8). (**D**) Clone size of TCR clonotypes, as classified in panel C and analyzed across 3 Rs (left) and 3 NRs (right) HNSCCs before or after neoadjuvant PD-1 blockade. Dots represent counts of individual TCR clonotypes, while boxes report 25^{th}-75^{th} percentiles with medians (horizontal bars).

Whiskers: min-max values; P values indicate significant comparisons calculated with two-tailed paired *t*-test (for persisting clones, pre vs post) or two-tailed unpaired *Welch*'s *t*-test. (**E**), Bar plots depicting overall intratumoral frequencies of CD8+ TCR-clonotypes with different primary phenotypes (T_{NExM}: blue, T_{Ex}: red) among total CD8+ TILs. TCR clonotypes are classified based on their detection in pre and/or post therapy biopsies as Lost (pre-specific), New (post-specific) or Persisting (detected in both pre-post samples). Values are shown for each 3 Rs and 3 NRs with pre-post therapy assessments. Based on their size, TCR clonotypes are further divided in singletons (lightest colors), doubletons (intermediated colors) or expanded (composed by >2 cells; darkest colors Data File S9). P values indicates significant comparisons for expanded TCR clonotypes, as calculated with two-tailed unpaired *Welch's t*-test (Rs vs NRs) or with two-tailed paired *t*-test (pre vs post). (**F**) Dynamics of Persisting or CD8+ TCR clonotypes with T_{NExM} (blue), T_{Ex} (red) primary phenotypes. Lines depict individual clones detected before (pre) or after (post) neoadjuvant PD-1 blockade within the TME of HNSCCs from 3 Rs (left) and 3 NRs (right). Bold lines report mean values. P values indicate significant clonal expansions or contractions, as calculated with two-tailed paired *t*-test.

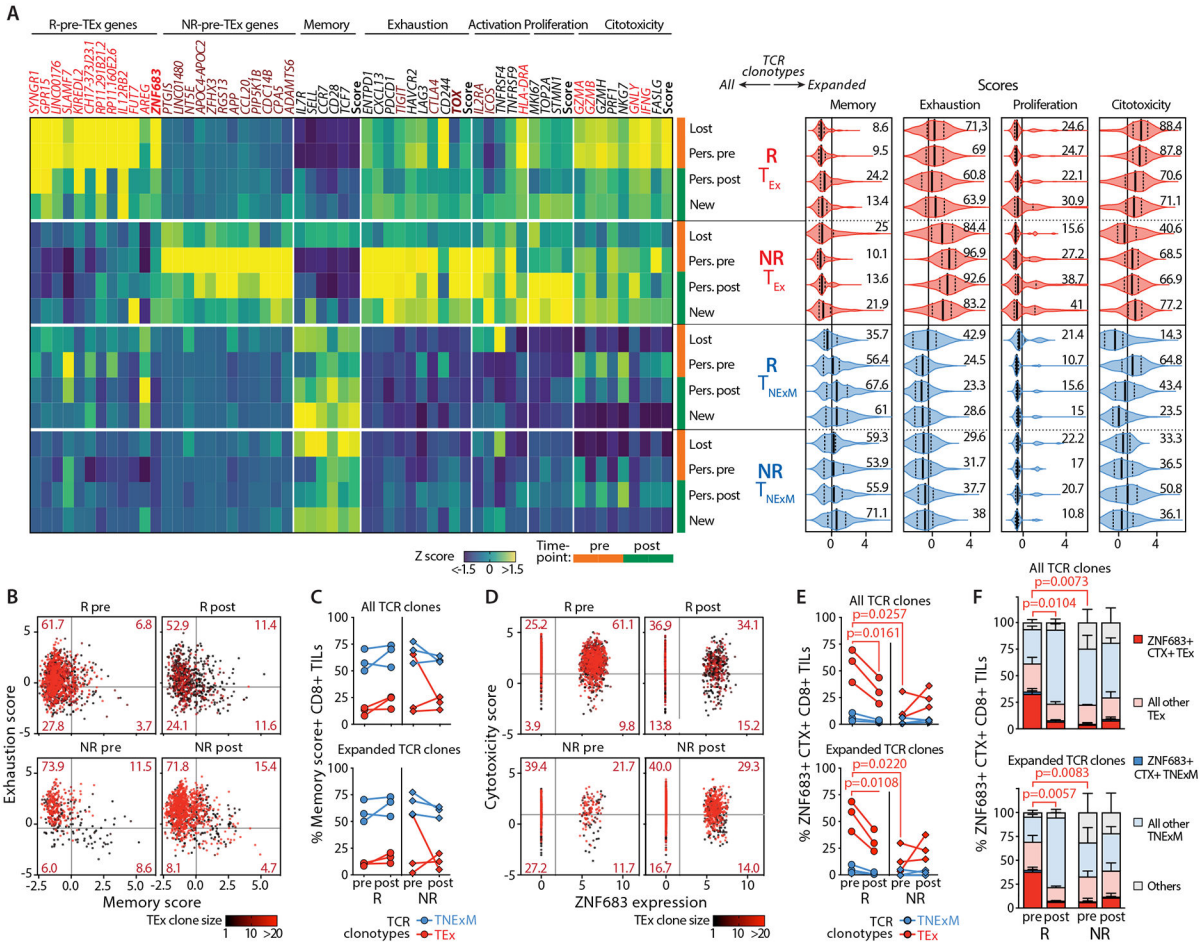

Fig. 7. High frequencies of ZNF683+ cytotoxic CD8+ TEx-TCR clonotypes associates with response to PD-1 blockade

(**A**) Phenotypes of clones Lost/New/Persisting TCR clonotypes. **A-Left:** Gene-expression profile of TCR clonotypes (rows) classified based on their primary phenotype (T_{Ex}, T_{NExM}) and divided based on their detection in pre and/or post-immunotherapy HNSCC tumors (Lost, New, Persisting [Pers.]) in Responders (R, n=3) or Non-Responders (NR, n=3). Average RNA-transcripts levels expressed as Z-scores are shown for i) top deregulated in R/NR-Pre-TEx signatures (see Data File S5); ii) for a panel of genes representative for T-cell related features; iii) for scores summarizing the expression of key genes (see Material and Methods). Genes enriched in R-Pre-T_{Ex} or NR-Pre-T_{Ex} signatures are labeled in red and brown respectively. Key transcriptional factors are highlighted in bold. Vertical tracks indicated evaluation of TCR clonotype in pre (orange) or post (green)-therapy timepoints. **A-Right:** Summary of the cell states of expanded (>2 cells) TCR clonotypes, divided by category (left). For each T-cell feature, scores summarize the expression of key genes (see Materials and Methods). Violin plots: median values (solid lines) with quartiles (dashed lines). Numbers: percentages of positive cells. Vertical lines: mean scores in the entire dataset. (**B,C**) Analysis of clonal revival in putative tumor reactive T_{EX}-TCR clonotypes. (**B**) Bidimensional plot depicting quantification of memory and exhaustion programs (scores) in T_{Ex}-TCR clonotypes detected in HNSCC biopsies collected before (pre) or after (post)

immunotherapy from 3Rs and 3 NRs. Dots represent single cells harboring TCRs with T_{Ex} primary phenotype and colored based on the size of each TCR clonotype. Thresholds: average score values across all CD8+ TILs. (**C**) The proportion of T cells with high memory score is quantified for each R (circles) or NR (diamonds), with lines connecting matched pre-post evaluations. Analysis was performed among all TCR clones (top) or expanded (>2 cells) TCR clones (bottom) with T_{Ex} primary phenotype (red) or within T_{NExM} clones (blue) as positive control (Data File S9). The lack of relevant differences in Rs and NRs documents that clonal revival is not significant in this clinical setting. (**D,E,F**) Quantification of ZNF683+ cytotoxic (CTX+) T_{Ex} cells among CD8+ TILs in HNSCC. (**D**): Bidimensional plot quantifying the expression of *ZNF683* (x axis) and cytotoxicity genes (summarized in a score, y axis, see Materials and Methods) in CD8+ TILs with T_{Ex}-TCR clonotypes, colored according to their expansion. Thresholds represents average values of variables, as measured in the entire dataset of CD8+ TILs. For each R and NR, the frequencies ZNF683+CTX+ TILs are reported in (**E**), among all (top) or expanded (>2 cells, bottom) CD8+ TCR clonotypes with T_{Ex} primary phenotypes (Data File S9) or among T_{NexM} clones as negative control (blue). (**F**) Quantification of ZNF683+CTX+ single cells across the overall CD8+ TILs. Bars: mean percentages with SEM. ZNF683+CTX+ TILs are shown with full colors amongst cell states classified as exhausted (red) or memory (blue). Grey: unclassified cells. Analysis was repeated for CD8+ TILs with any TCRs (top) or with expanded (>2 cells) specificities (bottom) (Data File S9). P values: significant comparisons calculated with two-tailed unpaired *t*-test (R vs NR) or with two-tailed paired ratio *t*-test (pre vs post).

Table 1:

Enrolled and treated patients and disease characteristic

Characteristic	All Patients (n=30)
Age at enrollment, y	
Median (range)	62 (30-82)
Sex, N (%)	
Male	19 (63)
Female	11 (37)
Ethnicity, N (%)	
White	28 (93)
Non-white	2 (7)
Smoking history, N (%)	
Ever	19 (63)
Never	11 (37)
Smoking pack-year history among Ever smokers[‡]	
Median (range)	21.5 (3-60)
Alcohol use history, N (%)	
Ever	14 (47)
Never	16 (53)
ECOG Performance Status, N (%)	
0	20 (67)
1	10 (33)
Tumor Site, N (%)	
Larynx/Hypopharynx	5 (17)
Oral Cavity	25 (83)
AJCC 8th Edition Clinical disease stage, N (%)[//]	
III	6 (20)
IV	24 (80)
Days Neoadjuvant pembrolizumab to surgery[†]	
Median (range)	40 (33-50)
Pathologic disease stage, N (%)[†]	
I-II	5 (17.2)
III	5 (17.2)
IV	19 (65.5)
Extranodal extension (ENE), N (%)[†]	
ENE+	4 (13.8)
ENE-	10 (34.5)
No Lymph node disease/no neck dissection	15 (51.7)
Surgical margin status, N (%)[†]	
Positive	4 (13.8)
Negative	25 (86.2)

Characteristic	All Patients (n=30)
High Risk Pathology (ENE+ and/or positive margin) Status, N (%)[†]	
High Risk	5 (17.2)
Not High Risk	24 (82.8)

[‡] 18 of 19 Ever smokers with pack-year smoking history data

[‖] All patients M0

[†] 29 patients underwent definitive surgery; 1 patient refused surgery